Benjamin Hofer BSc.

# Energy Harvesting with Printed, Ferroelectric Polymers

**MASTER'S THESIS**

to achieve the university degree of

Diplom-Ingenieur

Master's degree programme: Telematics

submitted to

**Graz University of Technology**

Supervisor

Ass.Prof. Dipl.-Ing. Dr.techn. Gunter Winkler

TU Graz, Institute of Electronics

Dipl.-Ing Andreas Tschepp

Joanneum Research, Institute of Surface Technologies and Photonics

Graz, August 2015

## AFFIDAVIT

I declare that I have authored this thesis independently, that I have not used other than the declared sources/resources, and that I have explicitly indicated all material which has been quoted either literally or by content from the sources used. The text document uploaded to TUGRAZonline is identical to the present master‘s thesis dissertation.

Date

Signature

# Abstract

The current developments in the electronic industry go clearly towards low power devices and expanding application areas. Trends like ubiquitous computing, wireless sensor networks and the "Internet of Things" call for a small and powerful underlying hardware on one side and capable power supply solutions on the other side. Of course, the energy obtained by the sun, water and wind is currently the most important alternative source for these devices, but other ways to obtain the necessary power receive increasing attention. Energy harvesting using piezoelectric material, i.e. converting mechanical into electrical energy, is a promising example for such a solution. New approaches, like using flexible, printed foils, can significantly extend the area of possible use cases and provide additional benefits.

The present work represents such an attempt by showing the potential for energy harvesting of a material called "PyzoFlex", developed by Joanneum Research. It analyzes and evaluates the material properties and behaviour to discuss subsequently the possible applications in the automotive field.

After dealing with the necessary parts of an energy harvesting circuit, a prototype of a batteryless tire pressure monitoring system was developed. During several test drives with this prototype it was proven that the output power of the used foils is sufficient to guarantee proper TPMS operation. Given the versatile properties of PyzoFlex, further developments including a simultaneous application as pressure sensor are conceivable.

# Zusammenfassung

Die derzeitige Entwicklung in der Elektronikindustrie geht eindeutig in Richtung von energiesparsamen Geräten mit immer weiteren Anwendungsgebieten. Trends wie Ubiquitous Computing, drahtlose Sensornetzwerke und das Internet der Dinge verlangen auf der einen Seite nach einer kleinen und leistungsfähigen Hardware als Basis und auf der anderen Seite nach einer geeigneten Energieversorgung. Die Energie erhalten aus Wasserkraft, dem Wind und der Sonne stellt zur Zeit die Hauptquelle für eine alternative Versorgung dieser Geräte dar, trotzdem erhalten andere Wege zunehmende Aufmerksamkeit. Energy Harvesting mit piezoelektrischen Materialien, d.h. die Umwandlung von mechanischer in elektrische Energie ist ein vielversprechendes Beispiel für solch eine Lösung. Neue Ansätze mit flexiblen, gedruckten Folien können dabei den Anwendungsbereich deutlich erweitern und zusätzliche Nutzen bringen.

Die vorliegende Arbeit stellt einen solchen Versuch dar, indem das Energy-Harvesting-Potential eines Materials names “PyzoFlex”, entwickelt von Joanneum Research, aufgezeigt wird. Dabei werden die Materialeigenschaften sowie das Verhalten dieser Folien untersucht und anschließend eine Anwendung im Automobilbereich diskutiert und umgesetzt.

Nachdem die nötigen Schaltung für ein Energy-Harvesting-System behandelt werden, wird die Entwicklung eines batterielosen Reifendruckmesssystem-Prototypen präsentiert. Während einiger Testfahrten konnte bewiesen werden, dass die Leistung der verwendeten Folien ausreichend ist, um einen Betrieb des Reifendruckmessystems zu gewährleisten. Die vielseitigen Eigenschaften von PyzoFlex machen eine weitere Entwicklung mit gleichzeitiger Verwendung als Drucksensor vorstellbar.

# Contents

# Introduction and Motivation

The public awareness of energy related issues has increased dramatically since the beginning of the 21st century. Accordingly, the European Union established ambitious climate and energy targets for 2020, including the raising of the energy produced from renewable resources to 20%. This has lead to increasing research and development efforts in many energy related areas ranging from 10MW wind turbines to novel battery solutions. Although the main renewable energy sources on the large scale still remain water and wind, other technologies contribute significantly by covering application areas with different requirements. For example, piezoelectric energy harvesting is an emerging technology which allows the conversion of mechanical vibrations into electrical energy. Since this source is obviously independent from the sun or the wind, it creates interesting new possiblities. Of course the achievable powers are quite low compared to other renewable energy sources. Nevertheless, with the development of new low power electronic devices, especially wireless sensor nodes, this technology offers a great alternative.

For this reason, the present work discusses the possibilities of piezoelectric material for energy harvesting. Doing this, the focus lies on a certain kind of printable, ferroelectric polymere foil developed by Joanneum Research. After a description of the state of the art in chapter 1 the properties and behaviour of these foils are presented in chapter 2 and chapter 3. The high flexibility of the foils and the relatively simple manfacturing process open a whole range of potential applications. These are subsequently presented in chapter 4, concentrating mainly on the automotive area.

A very promising use case for piezoelectric energy harvesters is a batteryless tire pressure monitoring system (TPMS). Therefore, the practical part of this work includes a prototype of such a system based on the given piezoelectric foils. First chapter 5 discusses the necessary energy harvesting circuits in general, whereas chapter 6 describes the specific case of the developed prototype system. It consists of the already mentioned foils mounted on a tire and a device to measure and transmit the voltage value of the storage capacitor. Furthemore, a TPMS developed by Infineon was used to demonstrate the practical suitability of the developed system.

Chapter 7 then presents the results of the test drives with this prototype. Since many insights into the behaviour and application of the used piezoelectric foils were gained, chapter 8 gives an outlook on the possible future developments.

# 1. Energy Harvesting with Piezoelectric Material

In this chapter a general approach to piezoelectricity is presented with a description of material classes and a subsequent focus on piezoelectric energy harvesting.

## 1.1. Piezoelectricity

The first demonstration of the direct piezoelectric effect was published by the Curie brothers in 1880 proving that mechanical stress on certain materials produces electrical charge. Initially this property was discovered using quartz crystals, cane sugar and tourmaline but many other materials followed. Soon after this discovery the inverse piezoelectric effect was mathematically deduced and confirmed proving that every piezoelectric material gets deformed by an applied electrical field.

The first application making use of this principle was the submarine sonar during World War I leading to an immense interest and further research of piezoelectricity. In the 1940s it was discovered that certain ceramics (e.g. barium titanate, $BaTiO_3$) have a much greater piezoelectric coefficient due to their ferroelectric nature. Ferroelectric material is always both piezoelectric and pyroelectric (charge generation in response to temperature change). These materials allowed the development of new devices such as piezoelectric transducers, igniters, actuators, sensors, generators and many more.

Today it is known that also natural materials like dry bone, silk and wood are piezoelectric. Furthermore, polymers (e.g. PVDF - polyvinylidene fluoride) have a piezoelectric coefficient several times greater than quartz. Since polymers do not have a crystalline structure, which is a common cause for piezoelectricity, a special treatment is necessary. The long chain molecules are mechanically streched and poled under high AC voltages to achieve the desired property.

The direct piezoelectric effect is also called generator effect, indicating that mechanical energy can be converted into electrical energy. Consequently, this property can be used for energy harvesting.

The research on energy harvesting with piezoelectric material started in the late 1990 and produced since then significant attention following a fast growing development. Examples

for commercial available products as well as currently active research areas are described in section 1.3.

## 1.2. Materials

This section presents an overview of different material classes possessing piezoelectric and/or pyroelectric properties.

**Natural crystals:** E.g. Quartz, tourmaline, topaz. These crystals occur naturally and were the first discovered piezoelectric materials and show a comparable weak effect.

**Synthetic crystals:** E.g. Langasite, gallium orthophosphate. Synthesized minerals with quartz-like properties were developed in the mid-nineteenth century. Almost all quartz crystals used today in electronic oscillating circuits belong to this group. Like natural crystals this group is without treatment piezoelectric and does not need to be polarized. Furthermore, some of them can withstand high temperatures over 1000 °C without loosing their piezoelectric property.

**Synthetic ceramics:** E.g. Barium titanate ($BaTiO_3$), PZT (lead zirconate titanate). This group belongs like the polymere group to the ferroelectric material. This has several implications. First of all, these materials are piezoelectric and pyrolectric, offering two transduction mechanisms for energy harvesting. Secondly, like ferromagnetic material, they loose their ferroelectric properties if a certain temperature, called Curie point, is surpassed. To achieve the piezoelectric behaviour a strong electric field in the order of kV/mm has to be applied. This process is called polarization. PZT is a very common representative of this group and can be doped with various other elements to obtain different piezoelectric constants.

**Polymers:** E.g. PVDF. Piezoelectric polymers are ferroelectric as well and have to be polarized. Moreover, copolymers such as PVDF-TrFE are used to increase the piezoelectric response.

## 1.3. Applications

Piezoelectric material can be used in various ways to harvest energy. The most popular design today are piezoelectric cantilevers, either in MEMS or on the macro scale. Great efforts in research were made to analyze the mechanical and electrical behaviour of such structures to optimize the energy output. Piezoelectric cantilevers have to be exited mechanically at their resonance frequency to produce the maximum power. This frequency depends on the mass and shape of the used device and is typically in the kHz range. Furthermore, many piezoelectric devices are made out of crystal or ceramics and therefore they have a relatively small size and are not very flexible. Nevertheless, many approaches

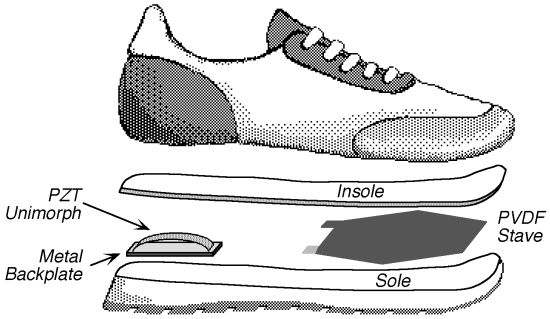


**Figure 1.3.1.** – Energy harvesting in shoes [19]

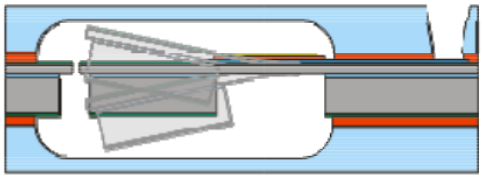

**Figure 1.3.2.** – Piezo cantilever in a MEMS [15]

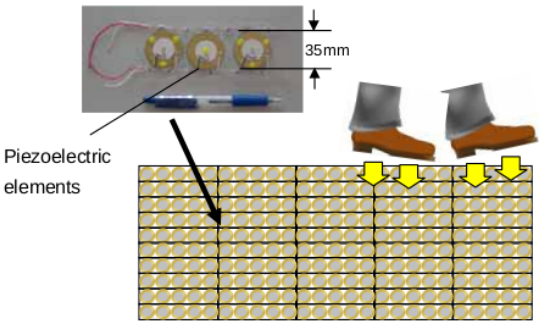


**Figure 1.3.3.** – Piezoelectric floor [9]

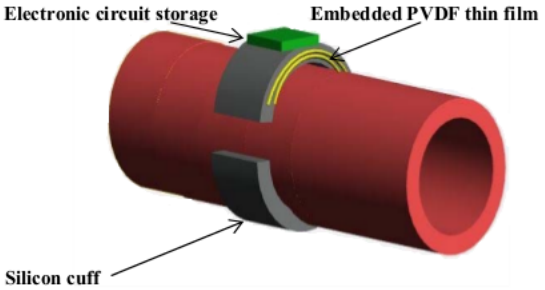


**Figure 1.3.4.** – Artery with piezo generator [13]

are possible to overcome these limitations e.g. using a flexible substrate where a thin piezoelectric layer is applied.

A less common mode is to use piezo elements to harvest energy from random or low frequency vibrations. Since the mechanical energy input is naturally much lower, the used devices are increased in size or applied over a greater area to compensate this disadvantage.

Following list of applications gives an insight into the areas of piezoelectric energy harvesting

- One of the first published examples was done 1998 by Kymissis et al. and analyzed the use of PZT ceramics and PVDF foils in common jogging shoes to harvest electrical energy (fig. 1.3.1) [19]. This energy was subsequently used to power an RF tag and send periodically an ID. The average power output of the used piezo generators was up to 1.8 mW.
- The NASA presented in 2005 a piezoelectric device that became later on the first commercially available piezo generator [1]. A ceramic piezoelectric wafer was sandwiched between an aluminium and steel sheet to produce a small amount of energy when it was plucked. A NASA spinoff created a wireless light switch based on this technology that needs no external energy source [32].
- A MEMS piezo generator based on PZT was published by Jeon et al. in 2005 [15]. It harvests vibrational energy with a cantilever design and has its resonant frequency at 13.9 kHz (fig. 1.3.2). The continuous output power amounts to 1 µW.
- Large scale piezoelectric generators are evaluated by the East Japan Railway Com-

pany at a train station in Tokyo since 2006 (fig. 1.3.3) [9]. A 6 $m^2$ floor area at the ticket gates was equipped with piezoelectric elements and produced 10 kWs of energy per day. However, the durability of the system posed a significant problem. A similar approch with piezoelectric floor tiles based on organic polymers (PVDF) is shown in [7].

- A very interesting application is discussed in [13]. A PVDF thin-film wrapped around a blood artery could harvest energy to power implanted devices such as a pacemaker (fig. 1.3.4). The reported power for the initial test setup was 16 nW.
- The increasing power consumption of electronic devices in todays automotive industry leads to another promising research area for piezoelectric energy harvesting. Maybe the most interesting application is a batteryless tire pressure monitoring system (TPMS). That is for two reasons. Firstly, the total necessary power lies in the capability of available piezo generators and secondly, it is not possible to connect the system to the on-board power supply via cables. The currently used batteries have a limited lifetime of a few years and cannot be replaced easily. [43] contains an example for a MEMS piezo generator developed for this task and additionally explains some general misconceptions about energy harvesting. [29] shows and compares different energy harvesting methods in car tires using PVDF and PZT.
- Finally, [40] can be mentioned where seven different commercially available piezoelectrical energy harvesters were tested for low frequency (2 Hz) operation. The reported maximum output power is 50 µW.

# 2. PyzoFlex

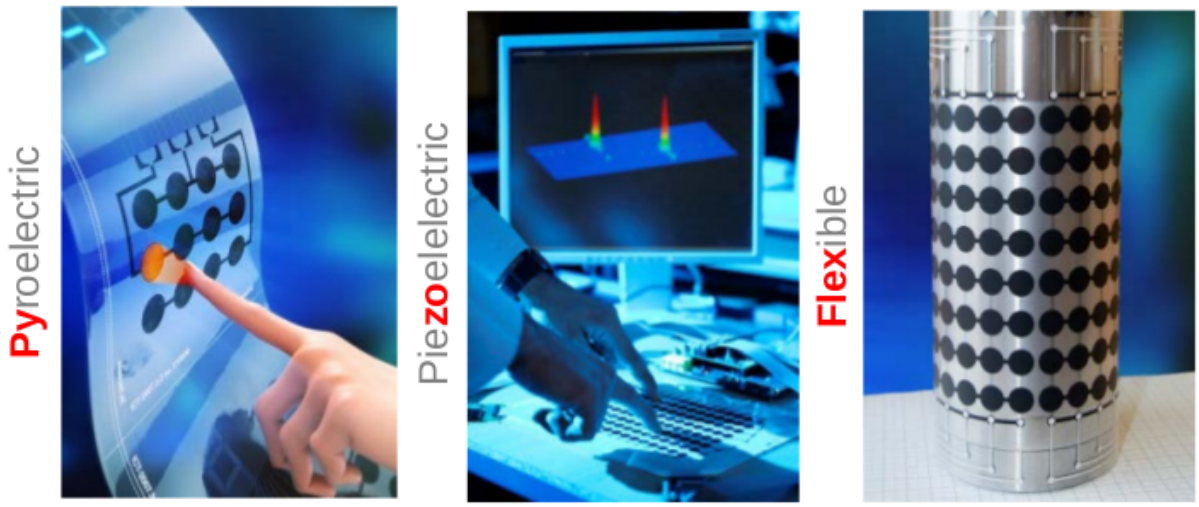


**Figure 2.0.1.** – Key properties of PyzoFlex [17]

In this chapter the general properties and current applications of the piezoelectric foils used for this work are presented. PyzoFlex was developed at the Institute of Surface Technologies and Photonics that is part of the Joanneum Research Forschungsgesellschaft mbH [17]. The name of the material is a composition of the three main properties: it is pyroelectric, piezoelectric and flexible.

## 2.1. Manufacturing

Two steps are necessary to produce a PyzoFlex foil. First of all the whole foil has to be created/printed and then a polarization step is necessary.

### 2.1.1. Printing

PyzoFlex is a sandwich composition of four layers: a substrate and three different inks. On the left side of fig. 2.1.1 the three ink layers can be seen, the right side shows a semiautomatic screen printer and the top a schematic how the inks are applied. Fig. 2.1.2 depicts a model of the finished foil, above with a single piezoelectric layer and below a two layer construction. The green layer in the middle is the piezoelectric ink, the top electrode is shown in black, the bottom electrode in blue. It is possible to add a

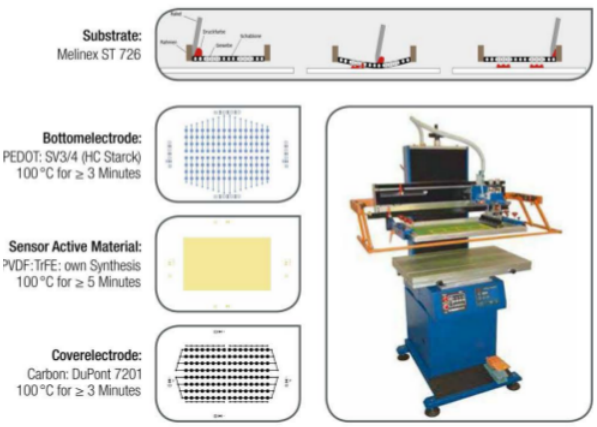


**Figure 2.1.1.** – PyzoFlex fabrication [17]

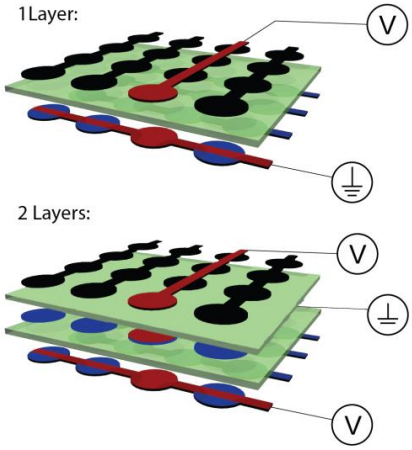


**Figure 2.1.2.** – Single and double printed PyzoFlex [48]

fourth conducting silver ink layer that can be used to print the tracks running from the electrodes to a common contact point. There the foil can be clamped into a connector to interface a PCB. Both figures show a foil design for a sensor matrix that was produced, but theoretically almost any two dimensional (or even stacked) design is possible. After every layer print a short annealing phase at 100 °C is necessary to guarantee the solvent evaporation. The only limitation is the screen printing resolution which becomes more important as the layer number increases. Like in every screen printing procedure the design of each layer gets transferred to a metal screen which is used to coat only the desired parts of the foil.

As substrate plastic foils with varying thickness, glass or even textiles are possible. For the purpose of energy harvesting during this work either 125 µm or 175 µm PET foils were used.

The piezoelectric ink consists of PVDF-TrFE (polyvinylidenefluoride-co-trifluoroethylene), a synthesized ferroelectric copolymere. Therefore the produced foils are sensible to temperature changes as well as mechanical stress and are able to produce electrical charge. The exact formulation of the printable material was patented by Joanneum Research. Like the other used inks this middle layer can be produced with varying thickness, though for the energy harvesting foils a uniform thickness of 5 µm was selected.

### 2.1.2. Electrical polarization

Since PVDF-TrFE is a ferroelectric polymere it has to be polarized to gain its piezoelectric property. This means to apply a high AC voltage of 140 MV/m and a frequency of 3 to 10 Hz between the top and bottom electrode to attain a permanent electrical polarization of the material. The applied electrical field aligns the prior randomly oriented dipols in one direction and creates thus the ferroelectric property. This alignment is stable unless the foil is exposed to temperatures above the curie point. For PyzoFlex this point lies at

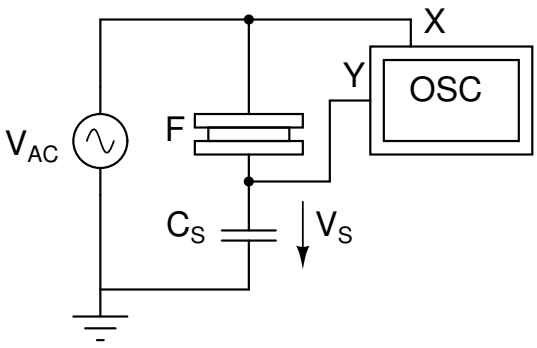


**Figure 2.1.3.** – Sawyer-Tower circuit

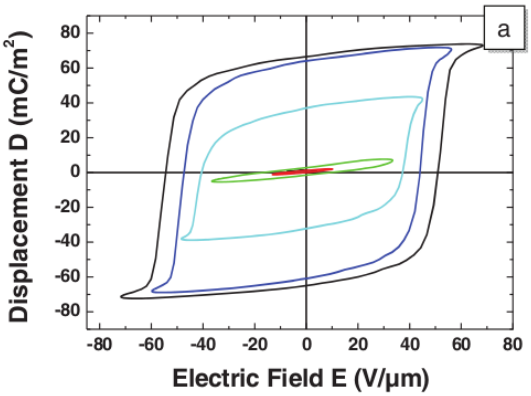


**Figure 2.1.4.** – Example hysteresis loops of PyzoFlex [49]

about 125 °C. If the material is cooled down and polarized again, the same ferroelectric behaviour as before can be obtained. The polarization of ferroelectric material can be seen as analogy to ferromagnetic material because they exhibit a similar hysteresis loop under the application of an electric field.

The polarization procedure is done with a Sawyer-Tower circuit (fig. 2.1.3), named after its inventors who used it in 1929 to measure the hysteresis loop of rochelle salt. The ferroelectric element $F$ is connected in series with the AC voltage source and a known capacitor. The voltage $V_S$ on this capacitor is connected together with the input voltage $V_{AC}$ of the circuit to a oscilloscope operating in XY mode. Since the capacities are in series they share the same charge $Q$ that can be calculated as $Q = V_S \cdot C_S$. This means that the sensed voltage $V_S$ indicates the charge on the ferroelectric foil. The polarisation $P$ can then be calculated as $P = \frac{Q}{A}$. The capacitor $C_S$ has to be selected accordingly to guarantee that most of the input voltage lies on the ferroelectric element. If the input voltage $V_{AC}$ is set on the x-axis and $V_S$ on the y-axis of an oscilloscopre a hysteresis loop can be observed. Fig. 2.1.4 shows an example of a recorded hysteresis loop produced by a PyzoFlex foil. The different line colors show the measured responses with increasing electrical field strength. The remnant polarization amounts to approximately 70 mC/m².

Due to the prior screen printing process it is possible that an unequal distribution of the polymere ink has caused short circuit connections between the top and bottom electrode. Through these connection flows most of the initial polarization current which melts the material locally and creates a high impedance spot again. This “self-healing” process is accompanied by neat sparks and does not have a significant influence on the polarization process or the subsequent operation.

More details about the fabrication process of PyzoFlex can be found in [49, 37, 48].

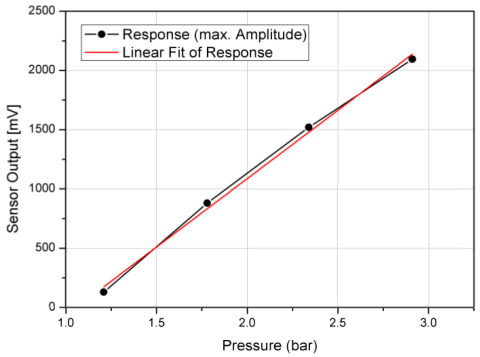


**Figure 2.2.1.** – Voltage response [48]

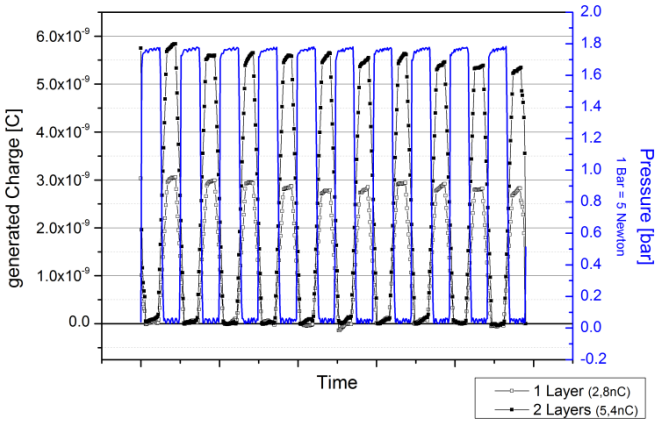


**Figure 2.2.2.** – Charge generation of double-layer Pyzoflex [48]

## 2.2. Material properties

Fig. 2.2.1 and fig. 2.2.2 show measurement results obtained by Zirkl et al. [48] in 2013. It can be seen that the voltage-pressure relation is very linear which allows an accurate pressure sensing. Therefore many applications involving touch, pressure or mechanical deformation of the foil are possible. However, since piezoelectric material only generates charge when being stressed, an absolute pressure measurement is not feasible.

Because of the ferroelectric nature of PyzoFlex the pyroelectric effect is another promising property. Although this could of course be an interesting topic for energy harvesting research, this work focuses on the piezelectric effect. A detailed description of the pyroelectric property of PyzoFlex can be found in [49].

Fig. 2.2.2 shows the charge response of two different foil designs. The active area was 1 $cm^2$ for the single and 2 $cm^2$ for the double layer foil. It can be seen that the generated charge doubles with the two layer design. During this work only single layer foils were used but according to this result it is obvious to try multiple layer prints to improve the generator power with little additional space.

**Figure 2.2.3.** – Almost transparent PyzoFlex [48]

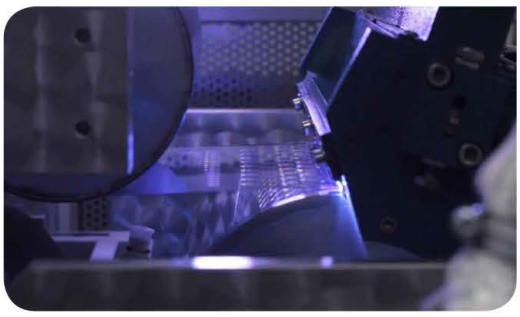

**Figure 2.2.4.** – PyzoFlex roll-to-roll production [17]

For touchscreens a invisible interface is vital and therefore an almost transparent form

of the polymere layer was developed. Fig. 2.2.3 shows an example for such a design with conductive silver lines running from the elctrodes to the foil connection points on the upper left and lower right corner.

Another evident feature is the flexibility of the foils. The printed material itself showed very good mechanical stability thus allowing a deformation in every direction. Again, this is very useful for e.g. novel input devices.

Finally the production costs should be mentioned. This is an important issue because energy harvesting devices have always to compete against generally cheap battery based solutions. Due to some factors PyzoFlex has the potential to be produced at very low cost:

- The piezelectric polymere can be printed on very large areas.
- Screen printing is a wide spread production technique.
- The relatively low temperature fabrication (100 °C) does not require much energy.
- Currently the printing of PyzoFlex foils with a roll-to-roll fabrication process is evaluated which would allow a high material output (fig. 2.2.4).

## 2.3. Applications

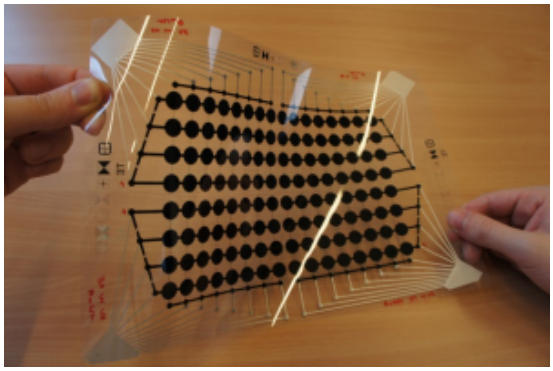

**Figure 2.3.1.** – Pyzoflex sensor matrix [17]

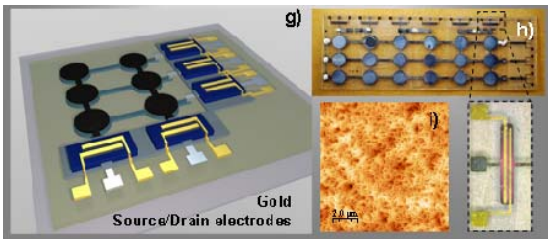


**Figure 2.3.2.** – Sensor matrix with OTFTs [17]

The most obvious and up to now most researched applications of PyzoFlex are located in the sensoric area. The biggest advantage of a pressure or temperature sensor of this kind is the ability to work without external power supply. To utilize this, a sensor matrix was developed that allows to detect multiple touches with a passive measuring method. Fig. 2.3.1 depicts this matrix. The black circles are the carbon top electrodes and printed silver tracks are used to access the electrode rows and columns. [48] deals with this application in detail and contains also a description of the processing circuit.

This development was taken already a step further towards a completely printable matrix sensor network by including organic thin-film transistors (OTFTs). Fig. 2.3.2 shows on

the left a schematic of such a matrix and on the right a photographic image with close up of the transistor.

Besides this application many others are thinkable and some of them are already under investigation:

- Robotics (artificial skin)
- Security (job safety, motion detectors)
- Life sciences (large-scale, medical diagnostics)
- ...

Until now not much research was done to verify the suitability of PyzoFlex for energy harvesting. Therefore the present thesis has the goal to analyze the piezoelectric material for this purpose and to develop a prototype that shows its potential.

# 3. Foil Characteristics

| Foil nr. | Area ($cm^2$) |
|---|---|
| 1 | 22 |
| 2 | 33 |
| 3 | 47 |
| 4 | 68 |

**Table 3.0.1.** – Area of foil patterns

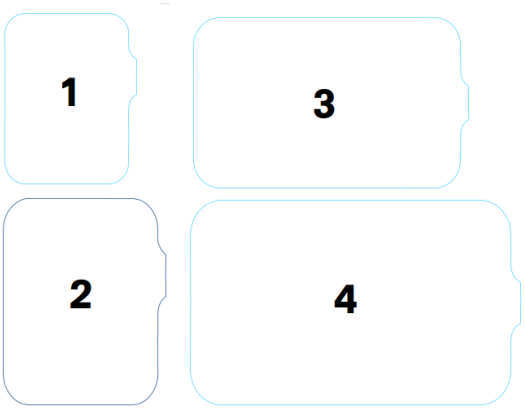


**Figure 3.0.1.** – Layout of foil patterns

This chapter discusses the electrical properties of the used PyzoFlex foils. Since the manufacturing process allows great flexibility in produced size and thickness of the foils it was necessary to define these parameters at the beginning. With an application in a car tire in mind four suitable piezoelectric layer patterns were selected, shown in fig. 3.0.1 and listed with their area in table 3.0.1. The thickness of the layer was kept uniformly at 5µm. The top and bottom electrode are printed respectively slightly larger in area underneath and on top of the shown patterns. In the used layer setup of the foil a conductive polymere was used as bottom electrode and carbon as top electrode. The substrate was a simple PET foil.

Foil nr. 1 and nr. 2 have their intended electrode contact points side by side (right side) whereas nr. 3 and nr. 4 on opposite sides (left and right side).

## 3.1. Equivalent circuit

The equivalent circuit shown in fig. 3.1.1 used as standard for a piezoelectric element applies also to the used foils. It contains a current source parallel to a capacitance and resistance. Table 3.1.1 lists the ranges of the circuit parameters that were encountered during the measurement and application of the four used foil patterns. This gives a general feeling for the magnitude of the foil properties, section 3.2 and section 3.3 deal with the respective parameter in detail.

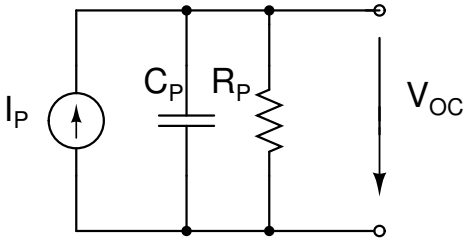


**Figure 3.1.1.** – Equivalent Circuit

| Parameter | Value |
|---|---|
| $I_P$ | $< 5$ µA |
| $C_P$ | 22 nF - 78 nF |
| $R_P$ | >500 MΩ |
| $V_{OC}$ | 2 V - 10 V |

**Table 3.1.1.** – Foil properties

For the following examinations the parallel resistance $R_P$ was neglected due to its very high value. This is common practice in the field of piezoelectric energy harvesting. [46] deals in detail with the equivalent circuit of a PVDF energy harvester and provides also a theoretical approach that includes a resistive or capacitive load.

## 3.2. Capacitance

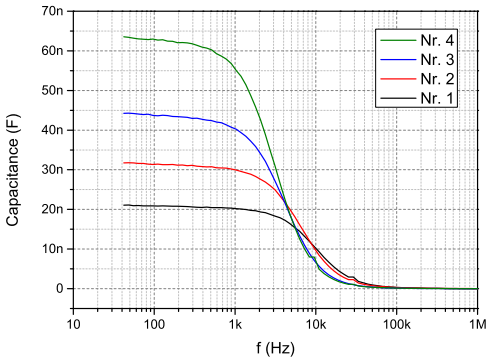


**Figure 3.2.1.** – Capacitance to frequency relation

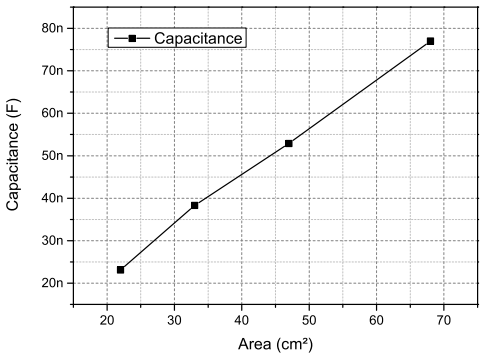


**Figure 3.2.2.** – Capacitance to area relation

Since the impedance of a piezoelectric foil is dominated by its capacitive part the capacity $C_P$ is of particular interest. Fig. 3.2.1 shows the behaviour of $C_P$ of all four foil patterns at frequencies between 42 Hz and 1 MHz measured with a Hioki 3532-50 LCR meter. It is clearly visible that the capacitance is very stable at low frequencies. Thus it is possible to see this parameter as constant for frequencies below 100 Hz where the aimed application will be located. Given that, the foil capacitance was measured henceforth with a HP 4261A LCR meter at 100 Hz where not otherwise noted.

Fig. 3.2.2 presents the relation between capacitance and area. For this diagram 3-8 foils of each size were measured and their capacitance averaged. As expected a linear correlation between area and capacitance can be observed with an average value of 1.1 nF/cm².

## 3.3. Current and voltage

Given the simple electrical equivalent circuit of fig. 3.1.1 without the resistance $R_P$ the open circuit voltage on the foil electrodes corresponds in the low frequency range (<50 Hz) to the voltage on the capacitance $C_P$.

$V_{OC} = I_P \cdot Z_C = I_P \cdot \frac{1}{j\omega C} = -I_P \cdot \frac{j}{2\pi f C}$

The generated current $I_P$ depends on the foil area, a larger active area creates a larger current. Ideally the relation between current and area is linear. Also an increased deformation frequency leads to an increased average current. Again this relation is ideally linear given an exactly similar deformation range. Furthermore, an increasing frequency leads to a decreasing impedance and thus to a lower open circuit voltage $V_{OC}$. However, together these two effects lead to a voltage $V_{OC}$ that remains stable during deformation frequency variations.

To analyze the behaviour of the given piezoelectric foils in practice a suitable test setup was used and is described in the following section.

### 3.3.1. Test setup

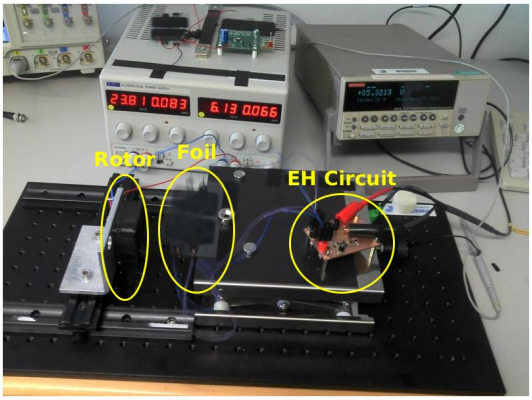


**Figure 3.3.1.** – Rotor test setup

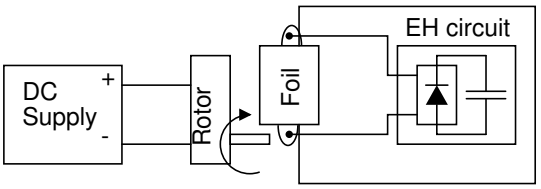


**Figure 3.3.2.** – Rotor test setup sketch

The key requirement in analyzing the motionelectrical behaviour of piezoelectric transducers is to provide a reasonable test setup to create a reproducible mechanical deformation. For the used foils such an appliance was constructed. Although it is far from being perfect it allows a simple and easy to use setup to satisfy this requirement. Fig. 3.3.1 and fig. 3.3.2 show and describe this so called rotor test stand. It consists of a small bolt mounted on a fan that is driven by a variable DC source. The piezoelectric foil is fixed on one side to a tray, the other side can oscillate freely as soon as the fan hits it once in its rotation. The connection of the cables leading to the foil electrodes is realised with rivets and cable lugs. Finally the cables connect to an energy harvesting circuit that consists of a voltage doubler rectifier with a following 10 µF MLCC. Fig. 5.2.4 depicts the circuit in detail, except for the capacitor the same components were used.

By varying the DC source voltage the rotation frequency of the fan can be controlled. Of course the achieved deformation was not completely constant since a higher angular velocity creates a significantly stronger impuls at the impact moment. Nevertheless, these variations were accepted to conduct some simple experiments.

Another source inconsistencies are the different sizes and masses of the used foils which posed a non uniformly fixation. E.g. the percentage of active versus total foil area was slightly different between the four foil patterns.

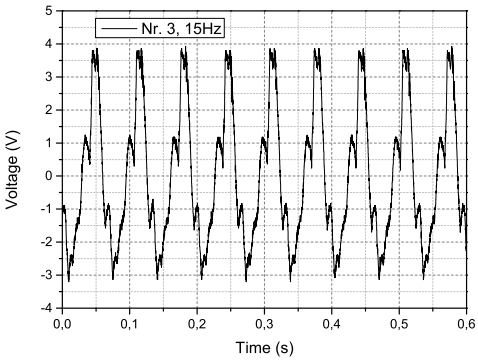


**Figure 3.3.3.** – Output voltage of foil pattern nr. 3 at 15 Hz

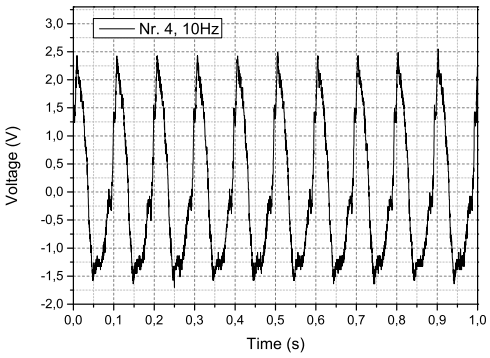


**Figure 3.3.4.** – Output voltage of foil pattern nr. 4 at 10 Hz

To test the behaviour of the chosen foil patterns different test configurations were used. The deformation frequency was set to either 5 Hz, 10 Hz, 15 Hz or 20 Hz. This was verified by measuring the voltage between the foil electrodes with an oscilloscope forming a load resistance of 1 MΩ. Fig. 3.3.3 and fig. 3.3.4 show examples of these measurements. It can be seen that the signals are not completely symmetrical due to the damped oscillation of the foils. Furthermore, the overall foil area was varied by using different foil patterns or a double stack of them.

## 3.3.2. Open circuit voltage

The open circuit voltage of the piezoelectric foil was determined indirectly using the voltage doubler rectifier circuit of the test setup. $V_{OC}$ corresponds to the sum of the maximum capacitor voltage and the diode forward voltage $V_D$ (0.2 V for the used HSMS280 [42]). Fig. 3.3.5 shows the capacitor voltage of the same nr. 2 foil at four different frequencies. Theoretically the voltage is not frequency dependendent, however due to the higher range of deformation it rises at higher frequencies. This comes from the greater acceleration and thus impact obtained by the rotor bolt.

This figure illustrates further that the time to charge the storage capacitor fully decreases obvoiusly as the deformation frequency rises. Moreover, the achieved voltage range is adequate to power standard electronic circuits e.g. microprocessors.

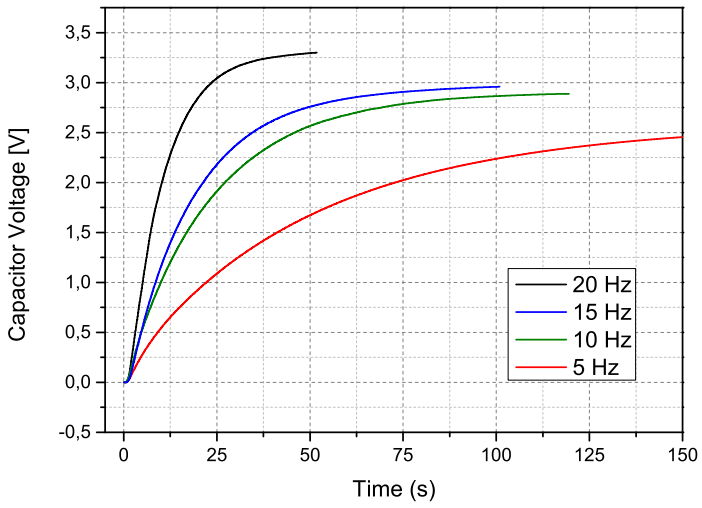


**Figure 3.3.5.** – Capacitor voltage at different frequencies

### 3.3.3. Charging current

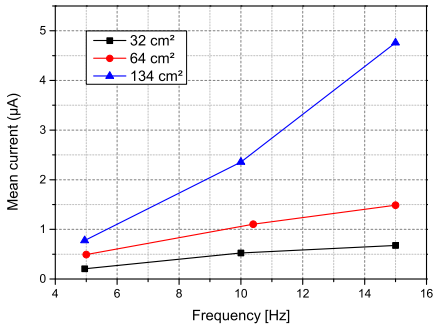


**Figure 3.3.6.** – Mean charging current over frequency

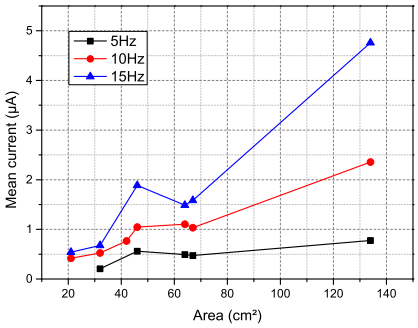


**Figure 3.3.7.** – Mean charging current over area

The charging mean currents produced by the different foils was calculated through total accumulated charge in the capacitor:

$$Q = U_C \cdot C, I_M = \frac{Q}{T}$$

$T$ is the measured time between 10% and 90% of the final voltage $U_C$ of the storage capacitor.

Fig. 3.3.6 shows the calculated currents of three different foil areas over the frequency range 5 Hz - 15 Hz. A linear correlation can be observed, however it is different for the used foils. This can be explained by the different size, mass and fixation of the foils.

Fig. 3.3.7 illustrates the relation between foil area and mean charging current. Again a certain correlation is indicated though significant deviations are present. It can be assumend that they derive from the issues described in the test setup (section 3.3.1).

## 3.4. Conclusions

After examining the discussions and test results in this chapter some important aspects regarding the application of the used piezoelectric foils can be pointed out.

1. To maximize the open circuit voltage and thus power output the ratio between active and total foil area should be as high as possible. This is because of the parasitic capacitance of the foil. If only a fraction of the total area produces current, it still has to charge the whole foil capacitance in order to increase the voltage between the electrodes. Therefore a large foil area should be parted and connected individually to a interface circuit if only a fraction of it gets deformed at the same time.
2. The bending or deforming motion of one whole foil should always be directed only in one direction. E.g. an s-shaped deformation of a foil would produce currents with opposite signs that cancel each other out.
3. It is obvious that a higher deformation frequency leads to a higher charge yield. For this reason a steady deformation with reasonable high frequency is a key requirement for a successful energy harvesting application.
4. Similarly an increased foil area leads to a higher charge production. However, the chosen foil area(s) should be in accordance with point nr. 1 and 2.
5. Since the foil capacitance plays a major role for the magnitude of the open circuit voltage it should be considered to change the foil properties (e.g. active layer thickness) to achieve a smaller capacitance and thus lower charge losses. Of course care must be taken to examine the influence of foil parameter changes to the charge production in order to prevent a counterproductive outcome.
6. Since the capacitor voltage rises to the maximum voltage on the input less the diode forward voltage(s), the by the foil produced voltage form is important for diode rectifier circuits. Peak-like voltages with the same mean DC value as more evenly distributed voltages allow to reach higher storage capacitor end voltages. This is because the voltage limit to start charging can be still surpassed when other more uniform voltages are already to low. However, the disadvantages for this situation have to be considered e.g. more losses due to the higher current peaks ($P_L = I^2 \cdot R$).

# 4. Possible Applications for Energy Harvesting

This chapter discusses the different possible applications of the given piezoelectric foils based on the foil characteristics presented in chapter 3 and chapter 2. Section 4.3 describes then the intended application for the developed energy harvesting prototype: a batteryless tire pressure monitoring system (TPMS).

## 4.1. General considerations

To find adequate use cases for the given piezoelectric foil it is helpful to review the main characteristics:

**Flexibility.** Due to the robust printing process on a substrate the flexibility of the foil depends almost only on the flexibility of the substrate. If a common PET foil with a thickness of e.g. 125 µm is chosen, the resulting foil is bendable with a very small radius in any direction.

**Scalability.** In theory the different applied layers can be printed to any extend. A successful roll to roll printing test done by Joanneum Research shows that large scale production is possible. However, for this work a semiautomatic screen printer was used which allowed a maximum size of A3 (297 mm x 420 mm).

**Lightweight.** The weight depends mostly on the used substrate because the printed layer thickness is in the order of only a few µm. Compared to other macro size piezoelectric elements this leads to a realtively low weight.

Additionally the pyroelectric property of the material has to be mentioned. Although this would extend the application area even further, it was left aside for this work because the focus was set on piezoelectricity.

Like in every energy harvesting application similar challenges have to be faced. E.g. very often the energy output is quite low so the field of use is reduced considerably. Following questions should be answered in order to find a suitable use case:

1. Is the generated energy output sufficiently high?
2. What devices can be powered with the produced energy?

3. Is there an energy source available that can be accessed easier?
4. Are the costs reasonable?
5. Is there an additional benefit by introducing the energy harvesting system?
6. Is the system robust enough for its aimed lifetime?

Considering piezoelectric energy harvesting and the given foils in particular the first two questions are the most critical. At low frequencies the output power is in the µW range and therefore there are not many applications where this would be sufficient. However, the IC development in the microelectronic industry goes towards always smaller structures leading to micro- and nanopower devices. Consequently, the more this trend progresses the more interesting become µW generators.

What regards question nr. 4 and 6: the cost and lifetime of the used foils are very promising compared to other piezoelectric materials. See section 2.2 for details.

Finally, the most interesting question is nr. 5. Since PyzoFlex foils can be used to sense mechanical stress, deformation, touch and temperature changes, many additional benefits would be possible.

There are in principle two different approaches to generate electrical energy with piezoelectric material. Both use mechanical vibrations, but the crucial point is the frequency of them. The most used way is to fix one side of the piezo element and to let it swing in mechanical resonance in order to receive the maximum energy output. This process depends heavily on the vibration frequency and the size/mass of the piezo element. The mass can be of course altered to achieve the desired swinging properties but when the vibration frequency varies the system runs at degraded performance. Nevertheless, this is still a viable solution. In [40] for example some off-the-shelf piezoelectric elements (cantilever designs) are compared for low frequency (2 Hz) operation.

The second approach is to design the system for random or low frequency vibrations. In this case the necessary mass and/or dimensions of a swinging element are not practicable and another way has to be chosen to receive an adequate energy output. Often the size or amount of parallel devices is increased e.g. with piezo elements integrated in walkways [9].

To operate the given piezoelectric foils in resonant mode either very high frequencies or an additional mass would be necessary. The mechanical adaption for this mode are of course feasible through using a stiffer substrate or attaching small masses. Then again, the valuable advantage of the high flexibility is left unused. Therefore most of the analyzed applications included the second approach of low or random vibrations.

This thesis was part of the so called ECO-touch project ([16]) wherein the application focus of a first energy harvesting protoype was defined as the automotive industry. Therefore the following section discusses this area in detail.

## 4.2. Automotive energy harvesting

Todays automotive industry is clearly about to be dominated by electronics and by the software running on the many electronic control units (ECUs) built into almost every vehicle. A current car model can have up to 100 ECUs. On one side the optimized driving process helps to reduce fuel consumption, but on the other hand the army of ECUs themself need more and more power to operate. The additionaly weight of all these devices alone poses a significant fuel consumption factor.

Therefore a great research and development effort is done to reduce the energy consumption or even recover energy. The most known and valuable measure is regenerative breaking for electric vehicles by making use of the kinetic energy. However, there is no other mechanism with a comparable energy output. Other less powerful methods use the car suspensions and shock absorbers.

On the small scale some interesting possibilities arise. Like known from the electrical component requirements the temperature range in automotive applications is extended from -40 °C to +125 °C. These temperature differentials could be used by thermoelectric generators (TEGs). Of course the energy output is compared to other sources in the vehicle very low and maybe only sufficient to power e.g. wireless sensors.

Another promising energy harvesting source are mechanical vibrations. This is is the primary application area for the piezoelectric foils used in this work. To achieve a high energy output, the useable area, deformation frequency and deformation extent needs to be maximized. Following list discusses some possible locations in a common passenger car.

**Suspensions.** Mounted somewhere between the spring and its bearing a foil area of 50 $cm^2$ to 75 $cm^2$ is possible. The deformation frequency lies between 1 Hz and 10 Hz and very high forces up to 100 kN are expected.

**Motor suspension.** A foil area in the same range is expected, the frequency is with 10 Hz to 30 Hz higher and the estimated force of 2 kN significantly lower.

**Drive shaft.** In this case a continuos rotatition is present. However, without special arrangements (e.g. attached extra mass) the deformation direction for a piezelectric foil is not favorable.

**Passenger seats.** At this location a comparable large area can be used. The disadvantage is a random and low excitation of an installed foil.

**Tire.** A common car tire (e.g. 205/60/R16, circumference 1900 cm) provides almost 2 $m^2$ of application surface and the deformation frequency at 100 km/h is 14 Hz.

Considering this list of possible locations the car tire is for several reasons the best option. First of all, it is a solution where promising use cases are present (pressure sensing, tire deformation measurement). Secondly it allows a comparably easy foil application and a

large deployment area. Therefore the realization of a batteryless tire pressure monitoring system was chosen as goal. This use case is discussed in the following section.

## 4.3. Batteryless TPMS

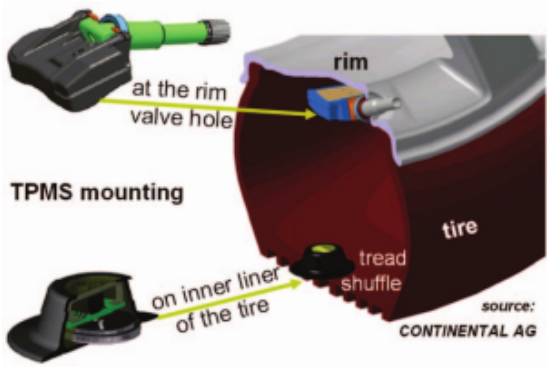


**Figure 4.3.1.** – TPMS mounting locations [47]

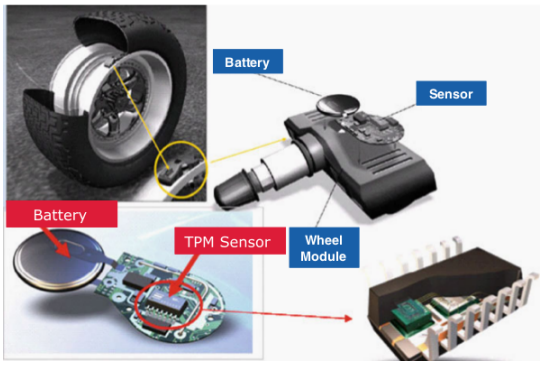


**Figure 4.3.2.** – Rim mounted TPMS [18]

According to the regulation (EC) 661/2009 of the European Parliament, since 2014 every new car has to be equipped with a TPM system, the US legislation already foresees this since the year 2000. The goals of this regulation is a reduction of fuel consumption and $CO_2$ as well as to improve safety. Consequently, the market and production volume of TPMS will increase significally and technology improvements will have a great impact.

Currently two different types are available: direct and indirect systems. While the direct TPMS resides inside the tire and provides a more accurate pressure measurement the indirect system comes generally at a lower cost. A piezoelectric energy harvester based on foils will be mounted inside the tire therefore this work focuses on direct TPM systems.

Fig. 4.3.1 shows two common locations to mount the pressure sensor system: either on the rim connected to the valve or directly on the inner tire running surface. Fig. 4.3.2 depicts a rim mounted system in detail with battery and sensor. A TPMS includes typically components to measure pressure, temperature, acceleration and supply voltage. An additional receiver and transmitter module allows the wireless communication with a base station.

There are a list of challenging requirements for these systems:

- Low power consumption to increase battery lifetime, 7-10 years are desireable.
- High shock resistance, accelerations of a few 1000 g are possible.
- Low size and mass. The total module should weight less than 10 g to prevent tire imbalance.

To fullfil these requirements the battery is normally not exchangeable, rendering the whole module useless if the battery is exhausted. Replacing this power source with an energy harvesting system based on PyzoFlex foils can have several advantages:

- A longer lifetime because battery exhaustion is impossible.
- Shorter measurement cycles due to more available energy.
- Additional sensor functionality (e.g. tire deformation).
- Less environmental impact. Batteries contain often toxic chemicals such as lithium thionyl chloride.

Of course the cost, temperature and mechanical stability of the piezoelectric foils are inevitable requirements to pose a real competition for a battery equipped system.

Until now considerable research work was done developing batteryless TPMS by using energy harvesting techniques, including electromagnetic and electrostatic harvesters, MEMS and macro size cantilevers [18, 29, 43, 44, 22, 45]. Only rarely a system based on similar flexible material as the piezoelectric foils used for this work is mentioned.

For further information on tire pressure monitoring system and a prediction for the future developments consider a recent study done by TNO and TU Graz in the year 2013 [41].

# 5. Energy Harvesting Circuits

In this chapter the general structure of the developed energy harvesting system is presented. The subsequent sections discuss the details and different implementation possibilites of each system block.

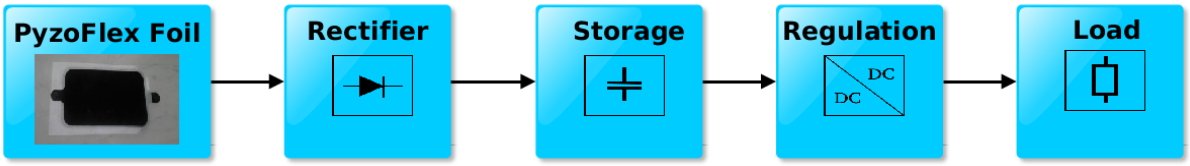


**Figure 5.0.1.** – Block diagram of the energy harvesting system

## 5.1. System Overview

Fig. 5.0.1 shows the general structure of the energy harvesting system developed in this work. The alternating voltage of the piezoelectric foil has to be converted into a usable DC voltage using an adequate rectification circuit. Then a storage element is needed because of the relative low generator power which lies in the range of µW. The following regulation block allows the conversion of the storage voltage into a useable level for the load. Furthermore, it has the task to control the load operation cycle depending on the available energy.

Each module has to be designed and fine-tuned according to the requirements of the overall system and properties of the other involved modules. These requirements and their implications are discussed in this section. Furthermore, section 5.2 to section 5.4 examine each of the components in detail.

Following by importance ordered list represents the main system requirements.

**High energy output.** The main goal of energy harvesting is to capture as much energy from the available generator element as possible. There are several possiblities that can be combined to satisfy this requirement. First of all, the choice of the rectifier circuit is crucial. Section 5.2 deals with this decision in detail. Given the relatively low energy output of the used technology the range of possible circuits is mostly limited to passive topologies, active rectifier circuits (e.g. using a microcontroller) would lead to excessive power consumption of the control circuit. The

next important possibility to increase energy production is the positioning and thus excitation of the piezoelectric foils. However, this is highly application dependent and is discussed in section 6.1.2.

**Low power consumption.** In order to provide the necessary energy to the load the harvesting circuit should use only a small amount of the collected energy. This requirement has a major impact on component selection as well as system structure and results in many tradeoff situations. Every additional component has to be evaluated if it justifies the additional power use.

**High load operation frequency.** Many practical applications of energy harvesting circuit foresee a load that measures or calculates something in time intervals of seconds or even minutes. Depending on the application this interval has to be below a certain time limit. For the first prototype of a batteryless TPMS a reasonable time interval was chosen to be below 60 s.

**Small size and mass of the electronic device.** This requirement is again application dependent and has to be considered in case of an electronic device mounted inside of a tire. The high acceleration and shocks occurring in this environement prohibit large and heavy components e.g. an inductor with high inductance.

This set of requirements were used to develop the prototype of a batteryless TPMS. For a more realistic and prolonged operation of such a device many more factors have to be taken into account. Clearly the mechanical robustness, temperature resistance and corrosion are the most important challenges to meet, others may arise during further research and development. However, the goal of this work is to show that such a system is in principle feasible with the given piezoelectric foils. Other requirements can only be handled if this can be proved first.

## 5.2. Rectification

This section presents some of the different topologies of rectifier circuits that were analyzed and simulated. Although there are many more approaches available, the requirements limit the possible solutions. The focus of the selection lied on the practicability and simplicity of the circuits.

The used simulation tool was LTSpice IV [12]. As long as otherwise stated, table 5.2.1 shows the parameters used for the simulations.

The properties of the piezoelectric foil equivalent circuit (current source in parallel to capacitance) were chosen according to an outcome of a prior test. In this test a nr. 4 foil was deformed manually with 1 Hz imitating the expected deformation on a tire running surface. During the exitation the short circuit current was measured with an SMU (National Instruments PXIe-4139). The result is shown in fig. 5.2.1. Consequently, a

sinusoidal current with equivalent DC value was chosen as input current for the simulation. Although this waveform is much more uniform than that of the measured current, it provides better understanding of the resulting voltages and currents of the circuits. The equivalent capacitance $C_P$ is the average capacitance of eight different nr. 4 foils.

| Parameter | Value |
|---|---|
| $I_P$ | 1.2 µA / 1Hz |
| $C_P$ | 77.07 nF |
| $C_S$ | 1 µF |
| Diode type | HSMS280 [42] |
| Simulation type | Transient, variable step width |

**Table 5.2.1.** – Simulation parameters

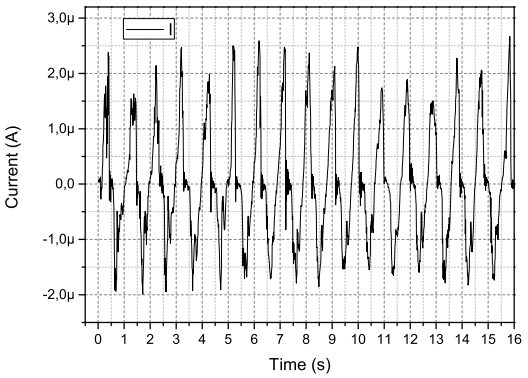


**Figure 5.2.1.** – $I_P$ measured at 1Hz manual deformation of a nr. 4 foil

## 5.2.1. Bridge rectifier

The bridge rectifier is the standard circuit to convert an AC into a DC voltage. It uses only four diodes to achieve this, thus presenting a simple and low cost solution. The upper part of fig. 5.2.3. shows the input and output voltage of the circuit. $V_{IN}$ varies between $V_{DC} + 2\,V_D$ and $-V_{DC} - 2\,V_D$ and $V_{DC}$ rises until it reaches the open circuit voltage of the piezoelectric element less $2\,V_D$. The lower part of fig. 5.2.3 depicts the currents through the diodes. If $V_{IN}$ surpasses $V_{DC} + 2\,V_D$ or falls below $-V_{DC} - 2\,V_D$, the diodes conduct crosswise (either $D_2$ and $D_3$ or $D_1$ and $D_4$) and current flows into $C_S$. Note that $C_S$ gets charged during every half cycle and that the power loss amounts to $2\,V_D \cdot I_L$. The maximum power occurs at half of the open-circuit voltage of the piezoelectric element. This is derived in [30] where also a more detailed analysis of this circuit, assuming ideal diodes, can be found.

## 5.2.2. Voltage doubler

A standard half-wave voltage-doubler circuit consists of an alternate voltage source, two capacitors and two diodes. If the voltage source is transformed into a current source, a circuit as depicted in fig. 5.2.4 results. The parasitic capacitance $C_P$ of the piezoelectric material takes the role of the first capacitor.

During the current sources negative cycle $C_P$ gets charged via $D_2$ only to the negative diode forward voltage $-V_D$. This means that the charge loss through the charge and

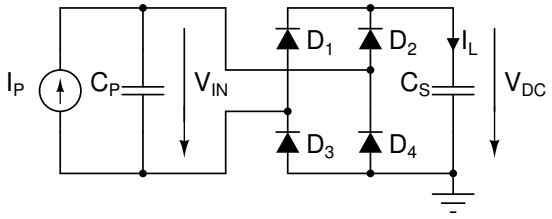


**Figure 5.2.2.** – Bridge rectifier circuit

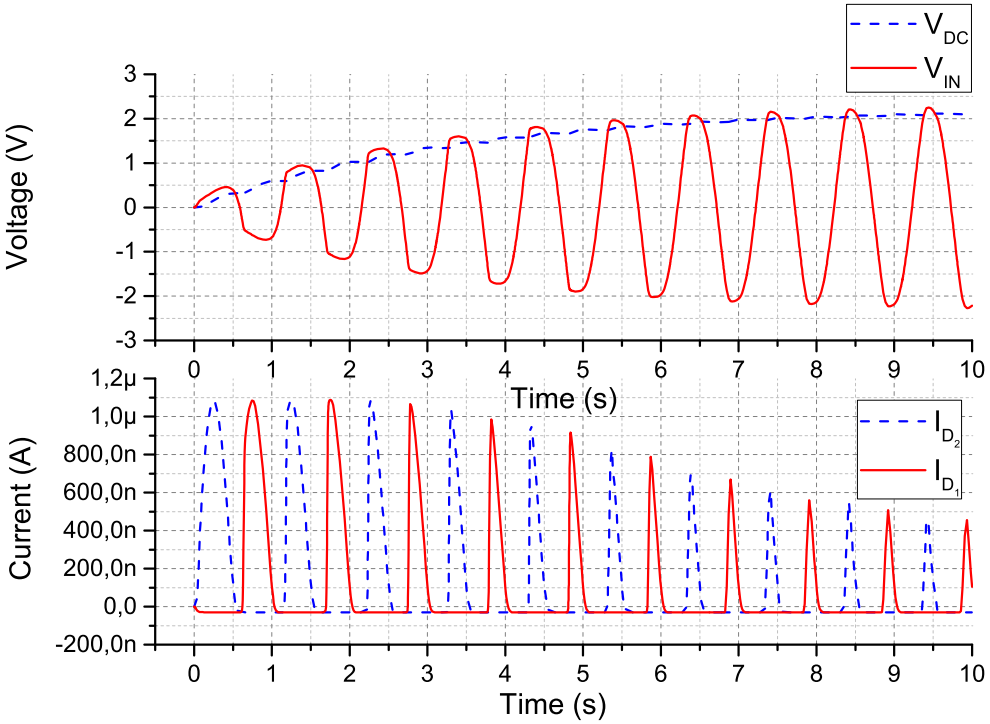


**Figure 5.2.3.** – Voltages and currents of BR

discharge of $C_P$ is reduced almost by the factor two compared to the bridge rectifier, where $C_P$ has to be charged to $-V_{DC} - 2\,V_D$. During the following positive voltage cycle $D_1$ conducts, $D_2$ blocks, the voltage on $C_P$ rises to $V_{DC} + V_D$ and current flows into the storage capacitor. Fig. 5.2.5 shows the simulated waveforms to clarify this process.

Compared to the bridge rectifier the input voltage $V_{IN}$ seems shifted to the positive by half of the peak-to-peak voltage. This allows the maximum voltage on $C_S$ to be twice the voltage as achieved with the bridge rectifier. Additionally the power loss is reduced, since during charging only one diode is active.

### 5.2.3. Synchronised Switch Harvesting on Inductor (SSHI)

This circuit topology was initally proposed 2005 by Guyomar et al. [14] and represents a non linear approach to achieve a higher output power. Since then different variations of this approach have been introduced and analyzed [20, 8, 23, 6]. The most commonly used is the parallel SSHI which was chosen to be discussed in this section.

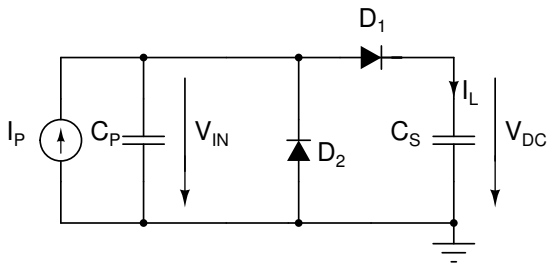


**Figure 5.2.4.** – Voltage doubler circuit

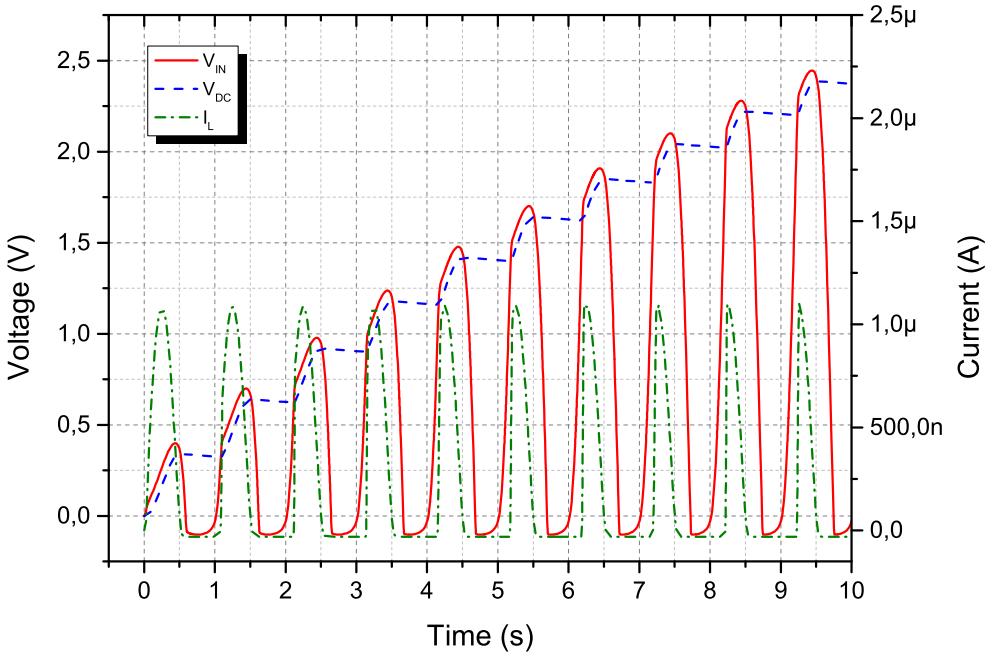


**Figure 5.2.5.** – Voltages and currents of VD

Parallel SSHI (fig. 5.2.6) uses a switching device and an inductance parallel to the piezoelectric element to increase the harvesting output power. Most of the time the switch remains open, but at every zero crossing of the current $I_P$ it closes for a short time period. At the same time the open circuit voltage on the piezoelectric element reaches its maximum, either positive or negative. By connecting the inductance $L$ to the parasitic capacitance $C_P$ a resonance circuit results. The switch closing time $t_c$ lasts for half of the oscillator period: $t_c = \pi \cdot \sqrt{L \cdot C_P}$.

During the short time of $t_c$ the voltage $V_{IN}$ abruptly changes polarity like depicted in fig. 5.2.7. The advantage for energy harvesting lies in the increased time available for charging the storage capacitor $C_P$ because the time to surpass the charging thresholds $V_{DC} + 2\,V_D$ and $-V_{DC} - 2\,V_D$ is significally reduced. A practical implementation of this circuit can produce up to 400% of the power produced by the bridge rectifier solution [14].

Nevertheless, the voltage inversion is even with an optimal switch timing not perfect, since the quality factor of the inductance and the power loss induced through the switch

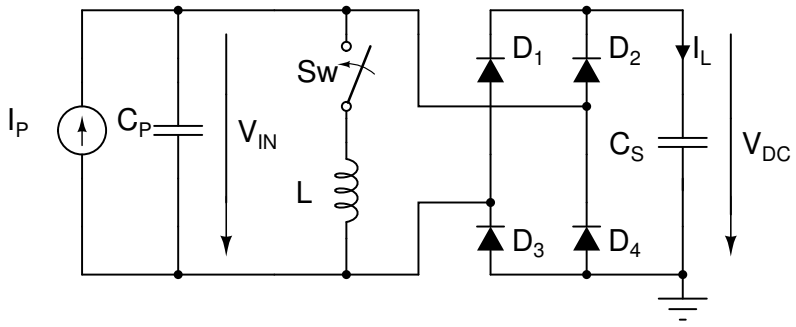


**Figure 5.2.6.** – Ideal P-SSHI circuit

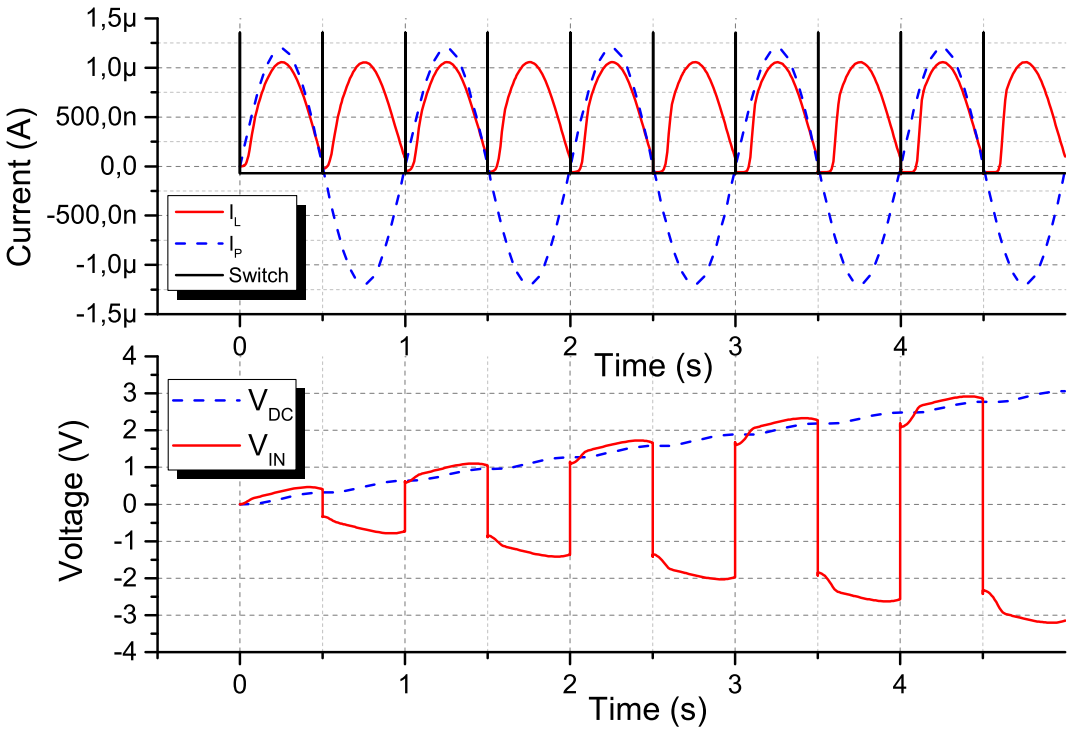


**Figure 5.2.7.** – Voltages and currents of ideal P-SSHI

have to be taken into account. This leads to a time period, shortly after the switching action, where the piezoelectric element has to increase the voltage without help to exceed the necessary voltage limits to charge $C_S$.

However, the increased ouput power comes at a cost that cannot be neglected. Several challenges have to be faced when applying this circuit practically.

- The switch has to be controlled, i.e. a control circuit has to decide the right moment to close and open.
- The used components have to be selected carefully. The inductance quality factor is an important parameter as well as the leakage current of all introduced devices.
- Mechanical limitations have to be considered, e.g. the mass of the inductance or the required circuit area.

- If more than one piezoelectric generator are used, each of them has to be connected to the switched inductance.

#### 5.2.3.1. Practical parallel SSHI circuit

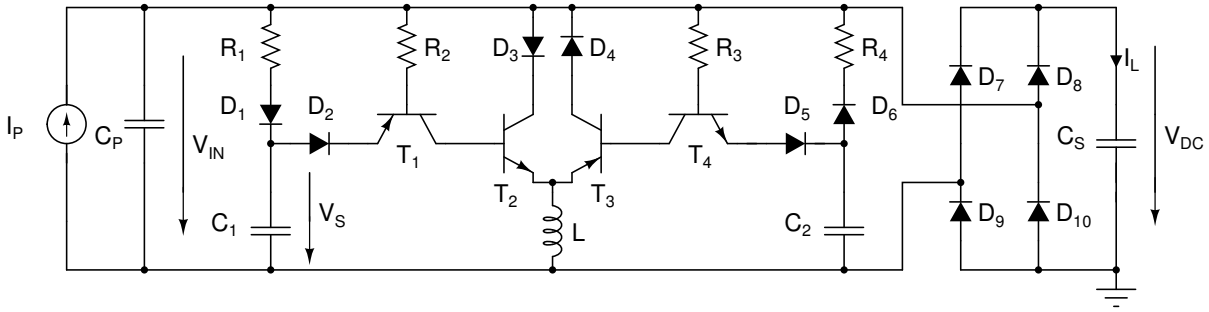


**Figure 5.2.8.** – Practical P-SSHI

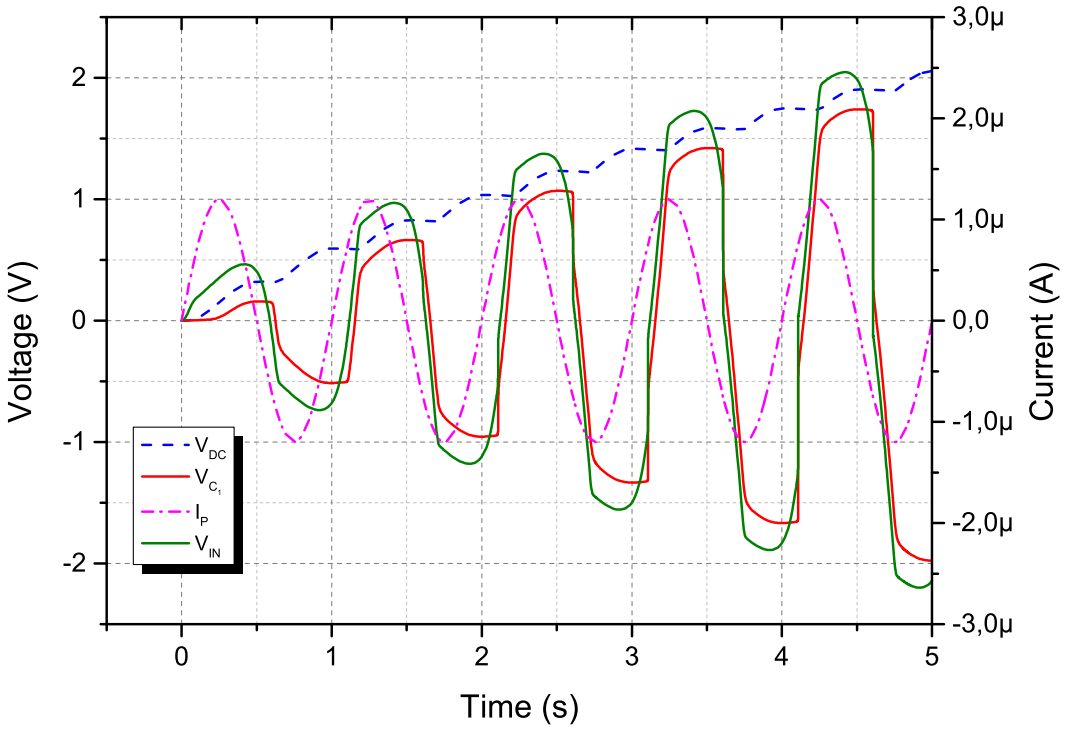


**Figure 5.2.9.** – Voltages and currents of practical P-SSHI

A practical circuit that performs the switch control is shown in fig. 5.2.8. It was patented 2007 by Richard et al. [36] and is presented together with a prototype in [21]. The working principle will be described in this section using only the left half of the circuit, since the operation is the same on the right part, only with different polarity.

The function can be splitted into three parts: an envelope detector formed by $R_1$, $D_1$ and $C_1$, a comparator composed out of $R_2$, $D_2$ and $T_1$, and finally a switch consisting of $D_3$ and $T_2$. When $V_{IN}$ rises, $V_S$ follows until $V_{IN}$ begins to fall again. If the difference between $V_S$ and $V_{IN}$ amounts to more than one diode forward voltage, the comparator

| Designator | Model/Value |
|---|---|
| $D_1$, $D_6$ | BAV199 |
| $D_2$, $D_3$, $D_4$, $D_5$, $D_7$, $D_8$, $D_9$, $D_{10}$ | HSMS280 |
| $T_1$, $T_3$ | BC857C |
| $T_2$, $T_4$ | BC847C |
| $R_1$, $R_4$ | 220 kΩ |
| $R_2$, $R_3$ | 10 kΩ |
| $C_1$, $C_2$ | 680 pF |
| $L$ | 10 mH, 37.4 Ω |

**Table 5.2.2.** – Component properties used for simulation

becomes active by means of a conducting $T_1$. This allows $T_2$ to connect the inductance $L$ to the piezoelectric element via $D_6$. The purpose of $D_6$ is to block the current path as soon as the current direction changes. Fig. 5.2.9 contains the simulation results of this process using the component models listed in table 5.2.2. The quite high time deviation of the switching moment from the zero-crossing point of $I_P$ is noteworthy. This is a major contributor to a lower power output than theoretically possible.

The advantages of this circuit are the autonomous operation and a simple design with only a few components. On the other side it has its limitations, mainly through the delayed switching created by the diode forward voltage gap, which poses a major problem. The effects of the switching time delay and inductor quality factor variations are analyzed in detail in [31].

It is noteworthy that this solution is only one out of a few that could be used to implement the SSHI technique. For instance, Qiu et al. [34] proposed another suitable self powered circuit. If the energy yield is sufficient, also a microcontroller based switch control could be considered.

### 5.2.4. Comparison

This section compares the three analyzed and simulated circuits in terms of output power and applicability for the given use case (tire pressure monitoring system). Although the used sinusoidal input signal for the simulations was chosen in the expected current range, it is crucial to remember that the piezoelectric foils can behave significantly different. Consequently, the conclusions of this examination can be only used as orientation; however, it is advised to test the rectifier circuits in a real test setup if possible. These differences could be e.g. a non uniform peak-like or even random excitation, a lower open-circuit voltage or long periods without any charging. The used simulation parameters were the same as in the single simulations (table 5.2.1, table 5.2.2) and as P-SSHI circuit the practical implementation described in section 5.2.3.1 was used.

Fig. 5.2.10 shows the voltage on the storage capacitor for each rectifier circuit. The differ-

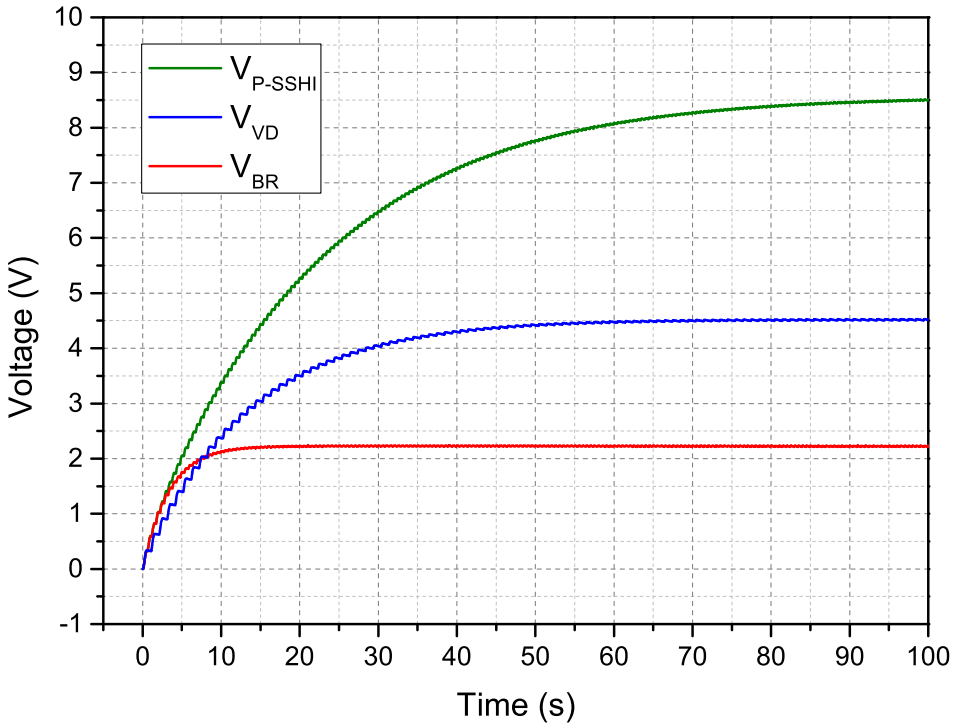


**Figure 5.2.10.** – Storage Capacitor Voltages

ences are clearly visible, P-SSHI produces more than 3.5 times of the final voltage as the bridge rectifier and two times the value of the voltage doubler. The reachable voltages are well within the useful range to power a standard electronic µC circuit.

Fig. 5.2.11 shows the maximum charging powers of the three circuits calculated from the storage capacitor voltage and the charging current $I_L$. When the capacitor voltage reaches the open circuit voltage of the piezoelectric element, the current flow should theoretically stop. However, in reality there is still a charging process ongoing to compensate the losses induced by diode and capacitor leakage. It can be clearly seen that the power is voltage dependend with one peak value per analyzed circuit. Because of their operating principle the voltage doubler and P-SSHI shift the maximum power point to higher voltages and extend thus also the operating range.

It has to be noted that the exact power value is only meaningful for the chosen input signal (sinusoidal, 1 Hz, 1.2 µA). Of course a higher deformation frequency and thus current can produce a higher charging power.

Given these electrical parameters it would be obvious to choose the P-SSHI circuit from the three possibilities to obtain the maximum charging power. However, in the practical application more factors have to be considered. The main limitation of the shown P-SSHI implementation is experienced when multiple input elements are present. Since the switch and inductor are located prior the rectifier part, every input element would need one of them. In theory it would be possible to share one inductor and have multiple switching

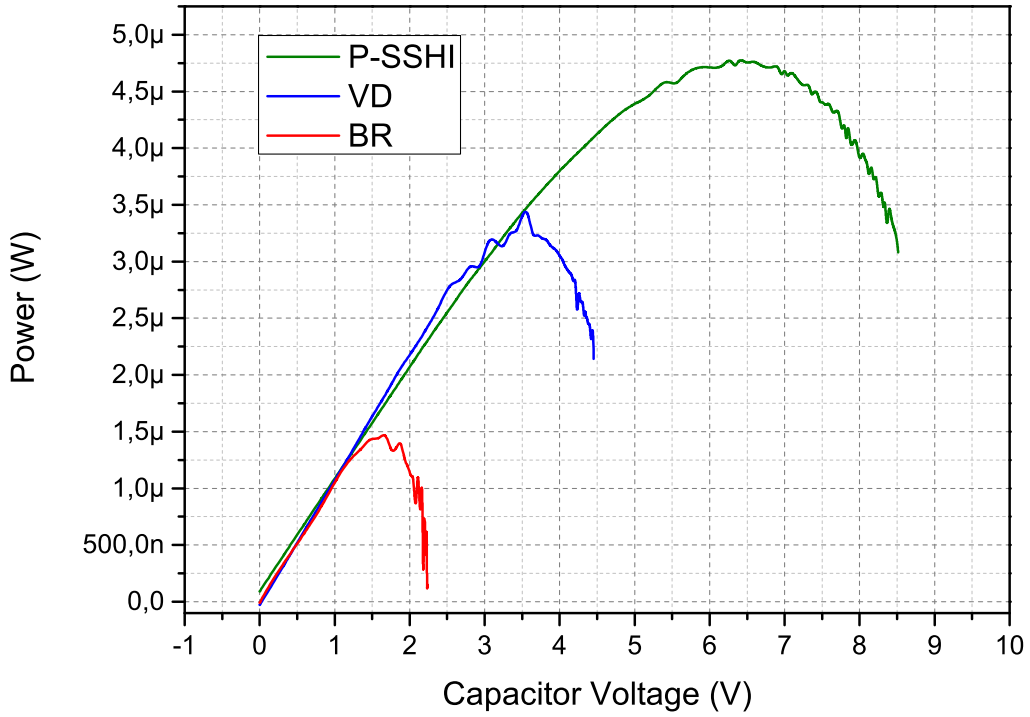


**Figure 5.2.11.** – Charging powers

devices, but that again would call for an arbitration mechanism. If a random excitation is expected, this issue becomes even more complex.

Another aspect that has to be treated is the amount of components needed for the P-SSHI solution. Many applications are not sensible to an increased circuit area and overall mass but there are some situations where these parameters are crucial. The in this thesis analyzed use case (TPMS) represents an example where e.g. the inductor mass would pose a major problem.

The voltage doubler has compared to P-SSHI a significantly lower output power. Nevertheless, it provides some considerable advantages over the other two circuits. It has the lowest component count, power loss and leakage current of the three analyzed circuits. Additionally it can share the same ground connection with the piezoelectric elements which comes in handy when many rectifier circuits work in parallel and only one common ground connection to the outside is necessary.

### 5.2.5. Component selection

Since the magnitude of the expected current signals ranges from nA to µA a proper component selection is crucial for the energy harvesting circuit design. Consequently, the overall target leakage current presents in the best case only a fraction of the average current flow into the storage element. This aspect becomes especially important when an

| Property | HSMS280 [42] | BAV199 [38] |
|---|---|---|
| $I_R(max)$ @70 V/25 °C | 200 nA | 5 nA |
| $I_R(typ)$ @10 V/25 °C | 10 nA | 3 pA |
| $V_F(typ)$ @1 mA/25 °C | 0.3 V | 0.8 V |
| $V_F(typ)$ @20 µA/25 °C | 0.2 V | 0.7 V |

**Table 5.2.3.** – Diode properties

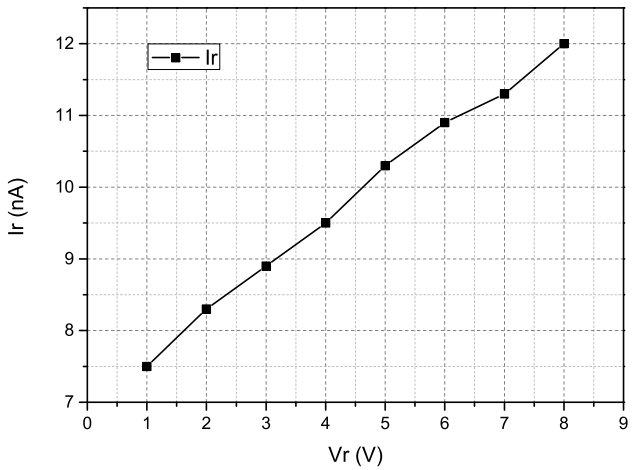


**Figure 5.2.12.** – $I_R$ of an HSMS2802 at 25 °C

extended time interval lies between energy harvesting and load activation. Furthermore, the maximum allowed voltage level for the interface circuit components has to be considered. Generally speaking, piezoelectric generators are capable to produce up to several hundred volts of open-circuit voltage. However, the used foils showed a maximum voltage below 10 V and thus this parameter posed no major restriction during the component selection process.

A choice that has to be made for every type of rectification circuit is the used diode type in order to reduce the power and charge loss. This consideration leads almost always to a tradeoff between leakage current and forward voltage. There are two major diode technologies which are usually used: shottky diodes or standard silicon diodes. Shottky diodes have commonly a lower forward voltage but in return a higher leakage current. Silicon diodes have the opposite properties, a higher forward voltage but lower leakage current. To give an example for components of each type table 5.2.3 shows two diodes with its key properties. The most important factor is in this choice the expected temperature during operation. At high temperatures a shottky diodes leakage current can rise up to 1000 times the value at 25 °C. For the HSM280 that is 10 µA at 100 °C [42], which is totally unacceptable. Regarding this paramater the silicon diode performs much better, max. 80 nA at 150 °C for the BAV199 [38].

Nevertheless, for the first prototype it was decided to use the HSMS280 since the expected temperature was estimated to be within an acceptable range. To get a feeling for typical

values for the leakage current an HSMS2802 diode was tested with a pA meter at room temperature. The result is shown in fig. 5.2.12.

When circuits with switched inductances are foreseen generally inductors with a high quality factor, i.e. low resistance versus inductance, have to be chosen.

Furthermore, the choice of the used energy storage is major topic and is therefore discussed in the following section.

## 5.3. Energy Storage

Due to the fact that the used piezoelectric foils have a relatively low output power it is necessary to harvest enough energy to intermittently perform a load operation cycle. This requires an adequate energy storage device as buffer between the interface circuit and the load or load regulation circuit. For the given application it was assumed that no long term energy storage is needed and thus the focus was on capacitors as storage elements. The general requirements are stated in the following list with our application specific values in parentheses.

- Low leakage current (<100 nA).
- Enough capacitance to store the necessary amount of charge (50-200 µF).
- Suitable operation voltage range (0-20 V).
- Ability to work in burst mode (20-50 mA)
- Small physical dimensions (<0.5 $cm^3$)

There are several different capacitor technologies that were analyzed against these requirements but already a few simple considerations lead to a viable solution for the intended application. Hence it is here avoided to go much into details, but rather the limiting factors of every technology are discussed.

**Supercapacitors** have a very high capacity in the range of farads, are physically relatively large compared to other capacitor types and have normally a cell voltage below 3 V. The leakage current lies in the µA range. Thus already more than one requirements is violated. The most unfitting parameter is the high capacity which would mean an unfeasible long charge time to reach a reasonable voltage. As example the datasheet of a gold supercapacitor can be used [27].

**Electrolytic Capacitors** are already a better solution with a capacity in the range of a few 100 µF, a working voltage range up to 50 V and a reasonable size. The application note in [35] from the capacitor manufacturer AVX investigates the suitability of different capacitors for energy harvesting. It concludes that tantalum capacitors are an adequate choice. However, these capacitors have leakage currents of several 100 nA as the datasheet of a recommended series shows [10].

**Multi Layered Ceramic Capacitors** represented the most viable choice. First of all, they have a very low leakage current of a few nA. Furthermore, the size-capacitance proportion is reasonable and operation voltages up to 16 V are even with high capacitance values of e.g. 22 µF possible. As example the datasheet of an appropiate choice can be found in [28]. The relatively small size (e.g. $3.2 \times 2.5 \times 2.0$ mm) allows the use of multiple capacitors in parallel with still resulting in an overall comparatively low volume.

To conclude this section it has to be mentioned that the storage element selection is highly application specific. If for example a high number of piezoelectric foils are used in parallel, which experience a steady and extended excitation, an electrolytic capacitor would be the better choice. For this reason there is no ultimate decision for what represents the best solution. Every case has to be considered individually.

## 5.4. Load Regulation

The last block in front of the load in the developed system is the load regulation. It has two main functions:

**Control.** Since an intermittent operation is foreseen, the activation and deactivation of the load power supply has to be managed in order to guarantee a proper load operation and energy efficiency.

**Voltage Conversion.** The voltage on the storage capacitor is very likely above the maximum operation voltage of a load device. It has to be assured that the voltage is converted with preferably low loss to a useable level.

To meet these requirements two different solutions were investigated.

### 5.4.1. Discrete threshold switch

| Designator | Component |
|---|---|
| $D_L$ | PLVA662A (6.2V) |
| $V_{REF}$ | ISL21080 (1.25V) |
| $COMP$ | TLV3961I |
| $R_1$ | 22 MΩ |
| $R_2$ | 11 MΩ |
| $R_3$ | 22 MΩ |
| $R_4$ | 3.6 MΩ |
| $R_5$ | 2.7 MΩ |
| $R_6$ | 12 MΩ |
| $T_L$ | BSH103 |

**Table 5.4.1.** – Used components

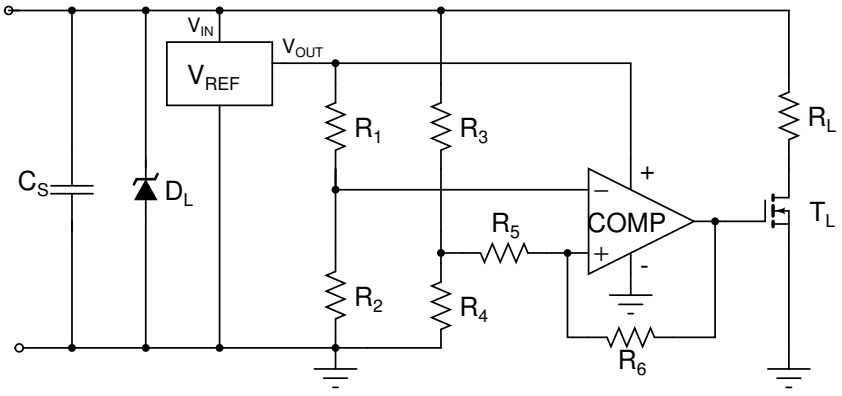


**Figure 5.4.1.** – Low current threshold switch circuit

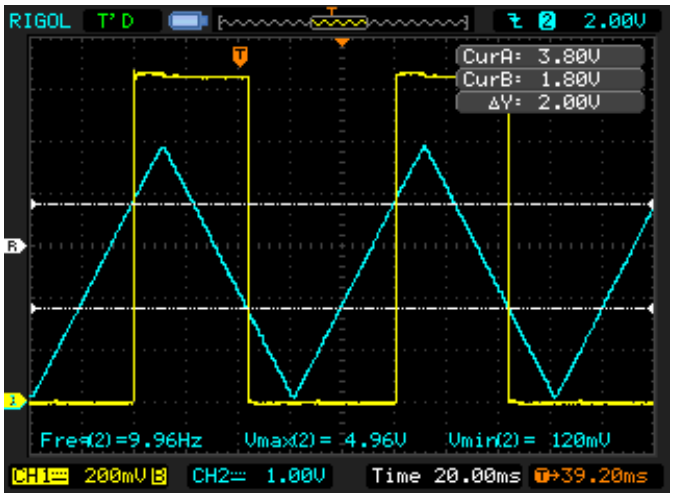


**Figure 5.4.2.** – Oscillscope plot of circuit test. CH1: load activation signal, CH2: input

The developed circuit shown in fig. 5.4.1 is a low current solution to regulate the operation of a load, depicted as $R_L$ in the figure. It works by using a comparator with stable reference voltage to switch the load on and off, depending on predefined voltage thresholds on the storage capacitor $C_S$. This comparator is supplied by a nanopower 1.25 V voltage reference and is thus independent of the varying input voltage. It works as non inverting comparator with hysteresis. Furthermore, $D_L$ limits the input voltage to 6.2 V to protect the voltage reference from overvoltage. In table 5.4.1 the used components for the practical implementation are listed. The resistor selection was done with a comparator hysteresis of 2 V as a target. This choice was done without any special requirement. Theoretically every threshold value between 1.25 V and 6 V is possible by adapting the resistor values. Moreover, the size of $C_S$ has to be selected according to the power requirements of the load to gurantee one operation cycle.

The typical current consumption is lower than 750 nA at 3.8 V. This is mainly possible through the low supply currents of the voltage reference (310 nA) and the comparator (150 nA).

A test with a voltage generator swinging from approximately 0 V to 5 V at the input

produced the results depicted in fig. 5.4.2 . Channel two shows the voltage at the base of $T_L$ that controls the load, channel one represents the input voltage.

### 5.4.2. Integrated load regulation solution

| Property | Value |
|---|---|
| Input quiescent Current | 950 nA |
| Input voltage range | 2.7 V - 20 V |
| Selectable output voltages | 1.8 V, 2.5 V, 3.3 V, 3.6 V |
| Max. output current | 100 mA |

**Table 5.4.2.** – LTC3588-1 key parameters

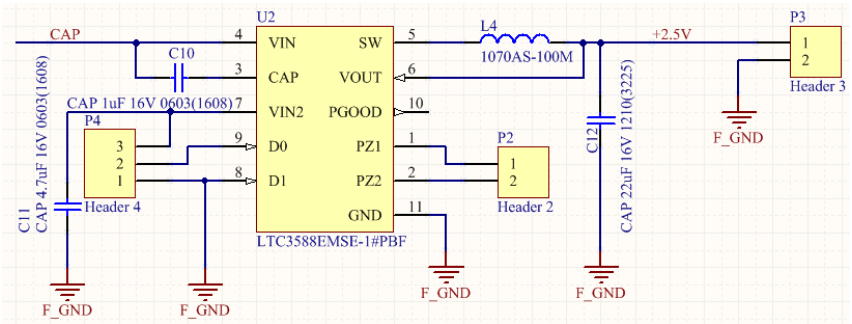


**Figure 5.4.3.** – Designed circuit

As an example for this type of regulator an integrated solution specifically designed for energy harvesting is discussed. The LTC3588-1 developed by Linear Technologies includes a bridge rectifier, a buck converter and necessary logic circuits to allow load management. It monitors the voltage on an external storage capacitor and begins to regulate to the selected output voltage as soon as a certain threshold voltage is surpassed. If the input falls below the required output voltage, the load gets disconnected again.

In [33] a kinetic energy harvesting application in a prostethic foot is presented as an application example for this IC.

Fig. 5.4.3 shows the circuit that was designed and used for the batteryless TPMS prototype. The "CAP" net comes from the storage capacitor and header 3 is the connection point for the load. Although the output is planned to be +2.5 V, header 4 allows to select also +1.8 V, depending on the selected jumper position. With this configuration the LTC3588-1 begins at typ. 4.04 V input voltage to provide power to the load. Header 2 interfaces the internal bridge rectifier and allows to connect a piezoelectric element. However, this feature was left unused for the prototype since more than one piezoelectric foil was used as input.

# 6. The Car-Tire Energy-Harvesting Prototype

To prove the capabilities of the used piezoelectric foils for energy harvesting a challenging use case was chosen: a batteryless tire pressure monitoring system (TPMS). The properties of the used material and their consequences described in chapter 3 have been analyzed together with the practical circuits discussed in chapter 5. The goal was to chose an appropiate system design for the given application. Section 6.1 presents the overall system with the considered constraints. Since the outcome of a first test was hard to predict, the practical verification was splitted into two phases: phase one described in section 6.2 served to determine the actually possible energy output of the harvesting device. Phase two builds on the results from phase one and contains a test system that uses a real TPMS. This is described in section 6.3.

## 6.1. System description

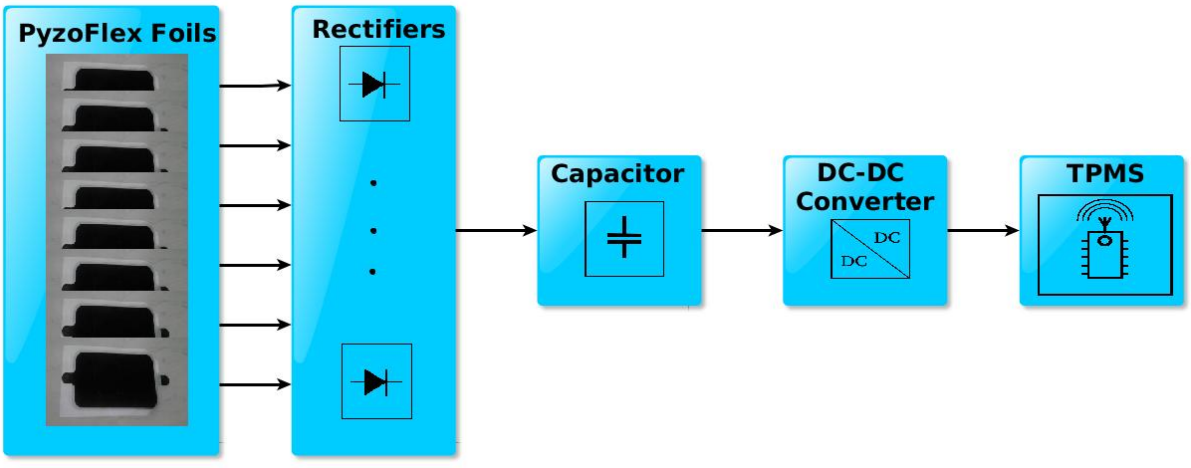


**Figure 6.1.1.** – Block diagram of the car-tire-energy-harvester prototype

Derived from the more general system diagram in fig. 5.0.1 the block diagram shown in fig. 6.1.1 represents the protoype structure for the batteryless TPMS. The main difference is the multiplication of the input elements to the storage capacitor. The implications of the test results for the achievable foil current and voltage in section 3.3 and the simulated efficiency for the rectifier circuits in section 5.2.4 are discussed in the section below.

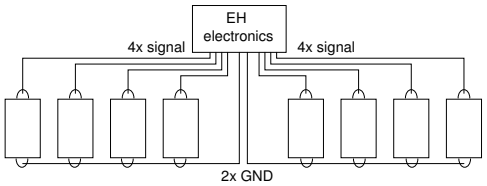


**Figure 6.1.2.** – Foil connections to electronics

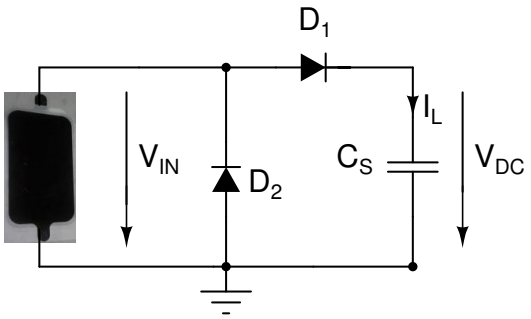


**Figure 6.1.3.** – Rectifier circuit for one foil

### 6.1.1. Foil size and amount

Since the produced current scales with the foil area at equal open voltage circuit (due to the likewise scaling capacitance) it is evident to choose a relatively large foil size. Because of the manufacturing process a new foil pattern design would be a considerable effort. Due to this reason the already available pattern were chosen as candidates. Foil nr. 4 is with 68 $cm^2$ the largest of the four patterns and was used therefore. The dimensions of it allowed an easy application to the tire inner running surface without any problems.

Provided that the first tire prototype represents always a certain risk and the outcome is especially in this application hardly to predict, it was decided not to use the full available area. With this in mind a tradeoff between effort and achievable energy output was chosen and a design of eight nr. 4 foils implemented. A previous estimation showed a charging time well below one minute for one TPMS transmitting cycle if all foils were active.

Fig. 6.1.2 shows how the foils were connected to the energy harvesting electronics. The design of the rectifier circuit allows to connect all bottom electrodes of the foils to a common ground.

### 6.1.2. Foil application and car tire prototype

A key problem to solve during the first practical tests is definetely the application and wiring of the foils inside the car tire to provide enough mechanical stability. To guarantee a close coupling between piezoelectric foil and tire deformation a special tire type was chosen: a 205/60/R16 ContiSeal produced by Continental [2]. This tire type has a special sticky coating on the inside tread to seal the tire in case of damage caused by e.g. a nail. Though this feature was not used as intended it provided an excellent hold for the foil on the inside running surface.

Two tire prototypes were manufactured with great help from the Joanneum Research team. The inside of the first is depicted in fig. 6.1.6 and shows two out of eight equally over the circumference distributed foils. The cables were connected via rivets and cable lugs to the foil electrodes. On the left side the bottom electrode connection and on the right side the top electrode connections can be seen.

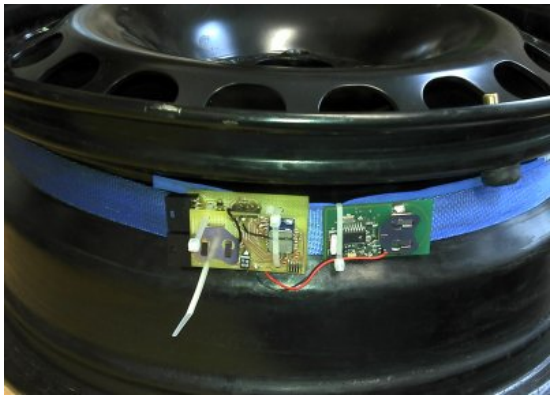

**Figure 6.1.4.** – Electronics mounted on the wheel rim

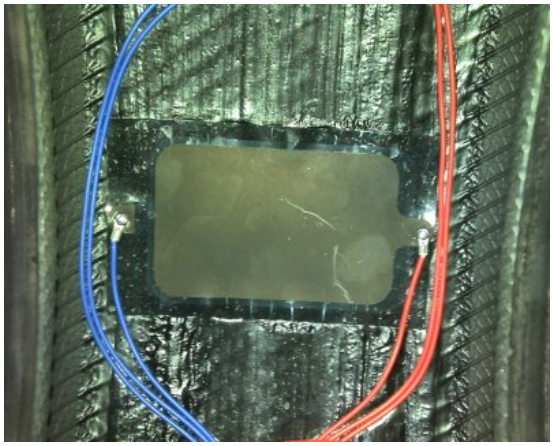

**Figure 6.1.5.** – Tire interior of V2.0

**Figure 6.1.6.** – Tire interior of V1.0

Due to the very high mechanical stress on the cables observed during the tests with version 1 the second version shown in fig. 6.1.5 used soldered cable lugs and screwed foil contacts. In both prototypes all the cable ends were layed to one common point where the connection to the harvesting electronics was done. Fig. 6.1.4 depicts the mounting of the electronics to the wheel rim with the harvesting and measurement electronics on the left and the TPMS on the right side. A simple tension belt and some cable binders produced very good results in fixing the electronics to the rim.

### 6.1.3. Rectifiers

As already pointed out in section 3.4 the ratio between active and total foil area should be maximized in order to reduce the parasitic capacitance and as a consequence receive a higher open circuit voltage. This leads to the requirement of separate charge paths for all foils due to the fact that in a rotating tire only a fraction of it gets deformed at a time. Therefore every foil needs its own rectification circuit.

As rectifier circuit a voltage doubler consisting of one diode pair was chosen. This very straightforward approach has several advantages:

- Both area consumption and amount of components are very low. This is an important benefit in case that each foil requires its own rectifier.
- The working principle is simple. No bulky inductances or synchronised switches are necessary.
- The achievable power output is according to the simulations sufficient. Although the achieveable power output is relatively low compared to other solutions, for a first prototype this drawback was accepted.
- Due to the working principle of this circuit the piezoelectric foil can share the ground connection of the storage capacitor

Of course the leakage current of the rectifier diodes increases with every additional foil and can be a major problem at a certain point. However, the used diode type (HSMS2802 [42]) showed an acceptable value at the expected temperature, like already shown in fig. 5.2.12. Thus the estimated total leakage current for the rectifier circuit lies below 100 nA.

### 6.1.4. Storage capacitor

The storage capacitor is a MLCC type with varying value depending on the test phase. This technology provides a very low leakage current, small size factor and a reasonable capacity up to 100 µF.

### 6.1.5. Voltage regulator

Given the requirements for a simple and reliable solution the LTC3588-1 from Linear Technologies was chosen [11]. There are several constraints that have to be considered. First of all, there is the quiescent current of up to 1 µA that in the developed circuit represents a constant load to the storage capacitor. Furthermore, the load managment grants not a high degree of freedom. The output voltage is together with the undervoltage lockout threshold fixed to a set of predefined values.

On the other hand the overall advantages from this solution prevail for a first prototype. Nevertheless, for a further development this system part could be significally improved by adapting it to the specific load requirements.

Like the TPMS this part of the system was not used until test phase two.

### 6.1.6. Tire pressure monitoring system

Thanks to the kind support of Infineon Technologies AG Developmentcenter Graz it was possible to use a fully-fledged TPMS for the car-tire-energy-harvesting prototype. Fig. 6.1.7 depicts a block diagram of the 14-pin IC. The system contains among other

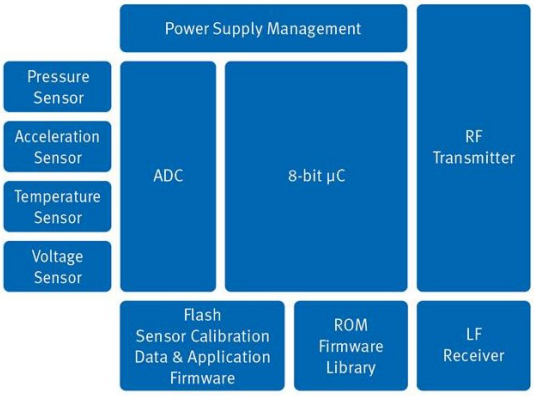


**Figure 6.1.7.** – SP37 block diagram [3]

**Figure 6.1.8.** – SP37 Demoboard with battery case

things four sensors, a µC, an ADC and an RF transmitter. It can measure the ambient pressure depending on the current temperature and send it over a dedicated 315/414 MHz FSK/ASK transmitter. The supply voltage range is 1.9 V - 3.6 V with a low standby current $< 0.7$ µA [4].

Fig. 6.1.8 shows the actual demoboard provided and programmed by Infineon that was used as TPMS. It was configured to measure every 10 s the ambient pressure and supply voltage and send it to a receiver module that was connected via USB to a PC. An also by Infineon provided software was used to log the transmitted frames on the PC.

Since this demoboard was presumably not intended to be applied in an actual tire it uses an antenna that is printed as a track on the PCB. Although this posed some difficulties in receiving the data frames it was still possible to log most of the sent data.

The power supply connections were realized by contacting the battery holder, no further change was applied to the demoboard. According to Infineon the total amount of charge necessary for one transmit cycle every 10 s including standby current is 85 µC.

## 6.1.7. Mechanical PCB setup

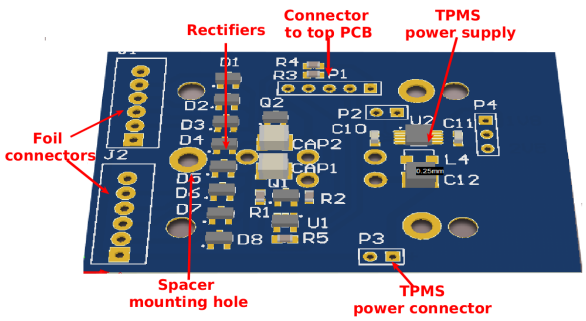


**Figure 6.1.9.** – 3D view of bottom PCB

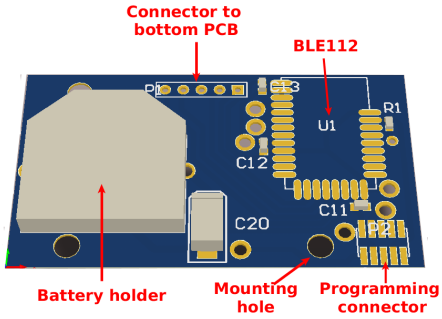


**Figure 6.1.10.** – 3D view of top PCB

The mechanical design of the electronics is composed of two parts: a bottom PCB, called energy harvesting module, holding the rectifiers, storage capacitors and TPMS power

supply and a top PCB with a battery supplied monitoring device. During test phase both parts were used as a stack, connected via a 5-pin header and fastened with cable binders and plastic spacers. For test phase two it would have been possible to mount the TPMS demoboard instead of the top PCB on the energy harvesting module and just connect the power supply lines. However, it was experienced that monitoring the storage capacitor voltage is a very valuable feature and thus the build-up was in the end the same for both phases except the added TPMS module in phase two (as shown in fig. 6.1.4). The details of the system for each phase are described in the following two sections.

## 6.2. Test phase one

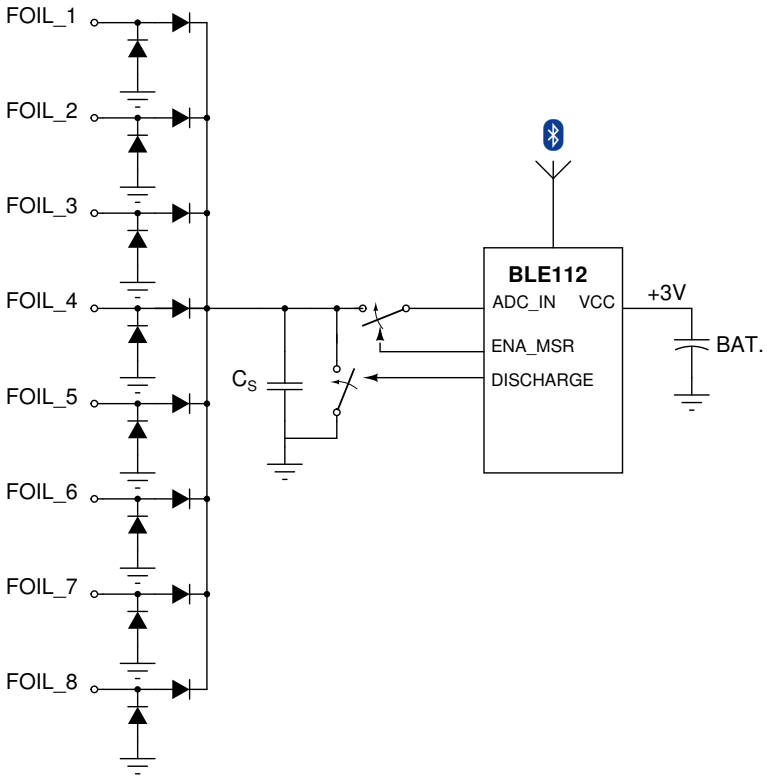


**Figure 6.2.1.** – Overview of the phase one system

The system for test phase one was developed to determine the energy output of the tire prototype equipped with eight nr. 4 foils (68 $cm^2$). This was done by measuring the storage capacitor voltage from which the harvested energy can be calculated. In order to aquire the measured data in the tire it is necessary to transmit it to the outside. This poses a major problem that every TPMS has to solve. Since a wire-solution introduces several new problems (e.g. tire or rim puncture, rotating cables) it was obvious to choose a wireless approach. Fig. 6.2.1 to fig. 6.2.4 show the resulting test phase one system in detail.

### 6.2.1. Overview

Fig. 6.2.1 represents an overview of the system. On the left the rectification part can be seen, comprising of eight voltage doublers. The cables coming from the foils were contacted via crimp connections to the two connectors located on the prototype PCB.

To measure and transmit the capacitor voltage value wirelessly a highly integrated bluetooth module was used. Thus it was possible to implement a measurement cycle with relatively little effort. This Module is located on the top PCB and supplied by a +3 V battery in order to not burden the storage capacitor. For this reason it is also possible to activate and deactivate the measurement path via bluetooth command.

### 6.2.2. Measurement and control

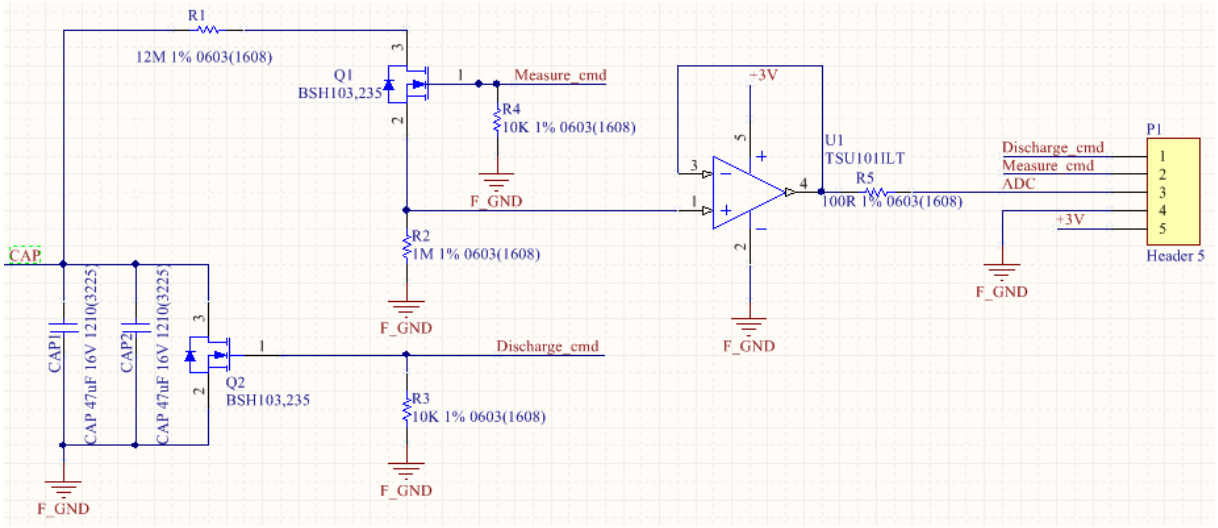


**Figure 6.2.2.** – Measurement and control circuit

The circuit design was done with Altium Designer 15.1 [24]. Figure 6.2.2 shows the exported schematic file of the energy harvesting module. The “CAP” net on the left side comes from the rectifier circuits and is connected to the storage capacitors plus terminal. The total capacitance shown is 94 µF. However, for test phase one only a value of 10 µF was used to reduce the charging time. 94 µF were used for test phase two to provide a large enough energy storage.

Via the “Discharge_cmd” signal the µC contained in the bluetooth module can short circuit the capacitor. This is a very useful feature to start a new charging cycle in case the whole prototype is already mounted in the car tire.

The voltage divider formed by $R1$ and $R2$ reduces the maximum expected voltage of 16 V down into the measurement range of 0-1.24 V. $Q1$ as well as $Q2$ is a low leakage n-channel MOSFET (max. 100 nA leakage current [39]) and serves to disconnect the voltage divider from the storage capacitor in case no measurement is ongoing. The source-drain voltage is very low due to the current in µA range and can be neglected.

The opamp $U1$ used as impedance converter is supplied by the battery residing on the top PCB. Header $P1$ shows the signals that are shared between the energy harvesting and the measurement module. Because of the pull down resistors on the MOSFET gate terminals it is possible to disconnect the measurement module and use the energy harvesting module as standalone circuit.

### 6.2.3. Bluetooth module


**Figure 6.2.3.** – BLE112 [25]

| Parameter | Value |
|---|---|
| Current Consumption | Transmit: 27 mA<br>Sleep: 0.4 µA |
| Supply Voltage | 2.0 V - 3.6 V |
| Digital I/Os | 19 |
| ADC inputs | 8 |
| Size | 18.10 x 12.05 mm |

**Table 6.2.1.** – BLE112 key properties

The requirements for the measurement and transmit part of the prototype are:

- Low influence to the energy harvesting module
- Reliable wireless transmission
- Low power consumption
- Easy implementation

The BLE112-A [25] developed by Bluegiga Technologies fulfills these requirements adequately and was chosen therefore. It is based on Texas Instruments CC2540 8051-type µC and provides many integrated features. The most important for this application are a 12-bit ADC, a fully integrated Bluetooth 4.0 low energy stack, a chip antenna mounted on the module and low power consumption. Furthermore, the module size is small enough to easily fit together with the 3 V battery on the top PCB.

The corresponding development board DBKLE113 with USB interface and on-chip debugger was used to program the module on the prototype.

Bluegiga developed for the provided modules an own script language called BGScript [26] that allows to implement comparatively easy and fast standalone software for the bluetooth modules. In addition, the software development kit (SDK) is completely free of charge and commonly available text editors can be used to write the necessary code.

Drawbacks of this solution are present but were accepted. Some examples are:

- Limited instruction set, this leads to sometimes rather cumbersome solutions.

- The power save states are selected automatically and cannot be initiated by the SW.
- Hardware settings cannot be controlled in detail, e.g. ADC aquisition time.
- Sometimes poor documentation of SW and HW.

Nevertheless, the BLE112-A poses a simple and sufficient tool for the given task. At this point it should be mentioned that the BLE112-A was preferred over the newer and more capable BLE113 because of the easier accessible soldering contacts.

#### 6.2.3.1. Schematic

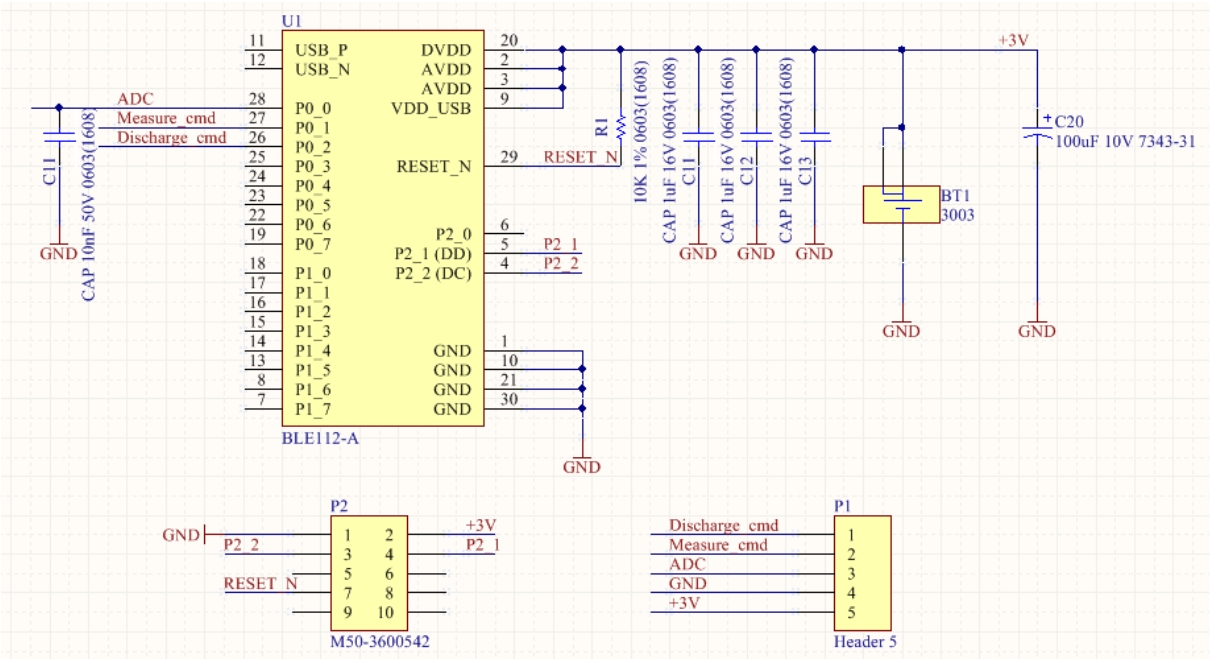


**Figure 6.2.4.** – Top PCB schematics

Fig. 6.2.4 shows the actual schematic of the top PCB containing the Bluetooth module. Port 0 holds the ADC input and the two digital outputs for controlling the measurement circuit. $P1$ represents the connector to the bottom PCB and $P2$ is the programming header. Since the module is programmable over I²C only few connector pins are necessary.

On the right side the +3 V battery connector is shown together with various decoupling capacitors.

### 6.2.4. Software

The software running on the Bluetooth module (client side) controls the measurement cycles and transmits data packages to a PC (server side) where the data can be gathered and displayed.

#### 6.2.4.1. Client side

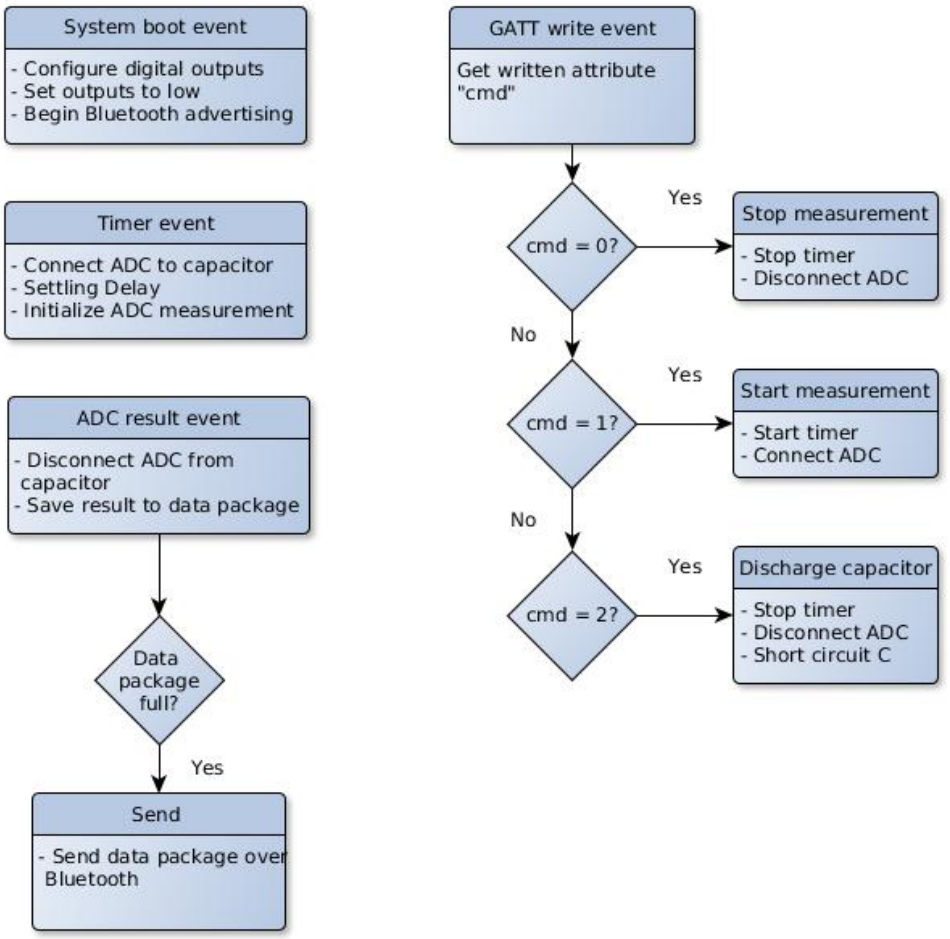


**Figure 6.2.5.** – SW block diagram

The propietary programming language provided by Bluegiga called BG-Script is of an event-driven type like e.g. Visual Basic. Consequently, the code execution starts when events such as timer overflows, a system start-up or interrupts occur.

Additionally a file for the Generic Attribute Profile (GATT) has to be generated where the provided services and attributes of the Bluetooth device are defined. This file can be found in appendix A.

Fig. 6.2.5 depicts a block diagram of the developed software that measures the storage capacitor voltage and sends it via Bluetooth to a Bluetooth dongle which is attached to a PC. The caption of the shown starting boxes describe the event that must occur to execute the associated code. There are four events that dominate the program:

**System boot.** At start-up the module initializes the digital outputs (short circuit capacitor, activate measurement) appropiately and begins the Bluetooth advertisment.

**GATT write.** If a connected device sends a command to the prototype by writing to the advertised GATT, this code part executes. The module checks which command was sent and acts accordingly. For example, to start the measurement, a “1” has to be

transmitted to the defined attribute and thus the module starts the ADC timer.

**Timer event.** At every timer overflow the voltage divider gets connected to the storage capacitor via the "measure_cmd" line (port 0, pin 1). Afterwards a delay loop is introduced to provide an adequate settling time. The timer is set to 100 ms for an ADC frequency of 10 Hz.

**ADC result.** If an ADC measurement was completed, the ADC-result event gets triggered. Then the voltage divider gets disconnected again to reduce the capacitor discharge and the measured value gets stored. If the data package size of ten values is reached it will be sent over Bluetooth. This amounts to one data package per second.

The complete code for this part is shown in appendix C

#### 6.2.4.2. Server side

The server side HW comprises of a specific Bluetooth dongle (BLED112), again developed by Bluegiga Technologies. An also provided free of charge graphical user interface (BLEGUI) can be used to communicate with the developed prototype.

With the default configuration following steps are necessary to work with the energy harvesting monitoring module:

1. Attach the connected USB dongle to the virtual serial port.
2. Start scanning with the default configuration. The Bluetooth device should then be detected.
3. Connect to the device and discover descriptors.
4. Write "0100" to the client characterstic configuration to activate continuous sending.
5. Write the desired command (0/1/2) to the attribute "command" to control the Bluetooth module.

Fortunately the Joanneum Research team provided a dedicated LabView program to handle this communication process much more comfortable.

## 6.3. Test phase two

### 6.3.1. Overview

In test phase two an actual TPMS was used to prove that with the given piezoelectric foils a batteryless TPMS is possible. Fig. 6.3.1 shows an overview of the system for this phase.

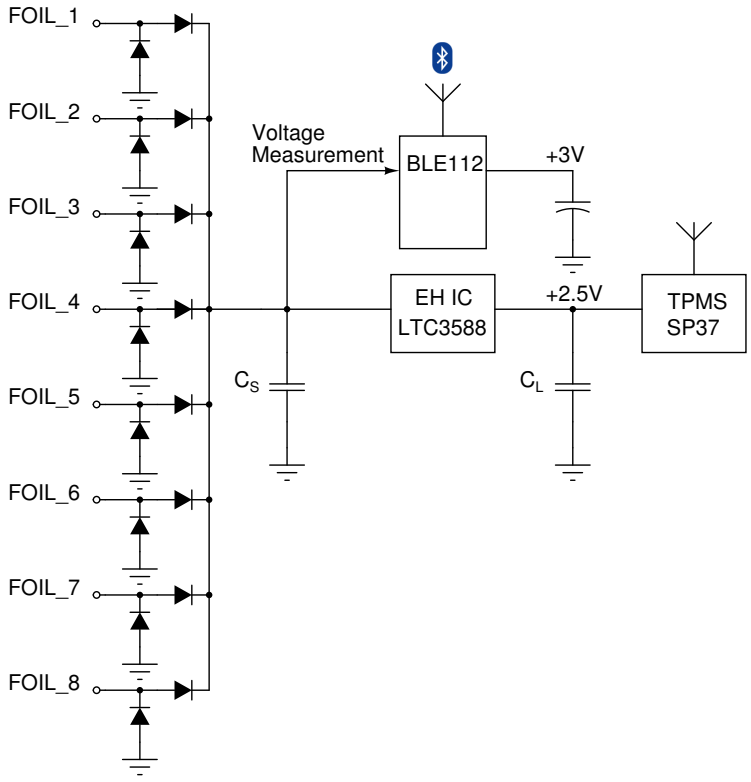


**Figure 6.3.1.** – System overview of phase two

Although it was not necessary, the capacitor voltage monitoring module described in section 6.2 was used again. The reason for this is that the antenna design of the TPMS demoboard did not allow a reliable wireless connection in all situations. It is assumed that this demoboard was not designed for an actual usage in a car tire but rather for software development in an office. If the voltage is monitored, the transmit action can be derived from the sudden drop during the sending in case the frame reception was not successful.

Like described in section 6.2.4.1 the software was designed to connect the voltage divider to the ADC only during the measurement period. This reduces the average load current for measurement to about 15 nA which can be compared with the leakage current of a rectifier diode [42].

## 6.3.2. Power Supply

The power supply and management for the TPMS was build on the LTC3588-1 IC from Linear Technologies [11]. Fig. 6.3.2 shows the developed circuit. The "CAP" net leads to the positive terminal of the storage capacitors and can be interrupted by a jumper. This allows to use the energy harvesting module without the power supply for test phase one. With header $P4$ the output voltage can be selected, with a jumper pin 2 and 3 were connected to set it to +2.5 V. The TPMS power supply lines were connected to header $P3$. $P2$ was not used for this setup.

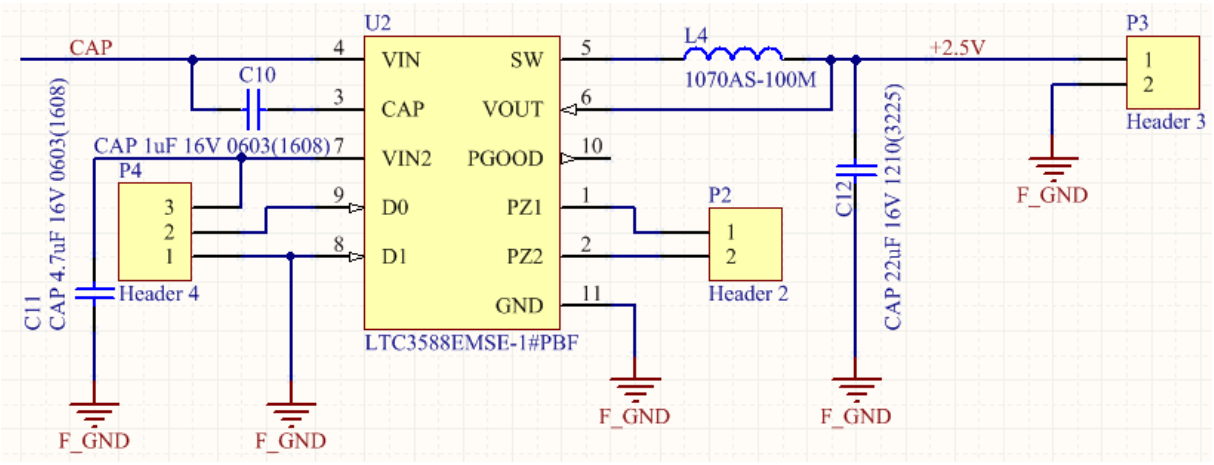


**Figure 6.3.2.** – TPMS power supply

The LTC3588-1 monitors the input voltage and starts regulating, as soon as it exceeds the under-voltage lockout threshold of typically 4.04 V. If the input voltage falls below the regulated output (+2.5 V), it disconnects the input again to stop further discharge. For further details of the LTC3588-1 see section 5.4.2.

In this test phase the storage capacitor size of the energy harvesting module was set to 94µC. Since the necessary charge for one pressure measurement cycle amounts to 85 µC, the voltage on the storage capacitor should fall from 4 V to 3.1 V. The remaining capacitor charge of 56 µC between 3.1 V and 2.5 V are certainly enough to compensate the expected losses.

### 6.3.3. TPMS module

The used TPMS module was a demoboard provided by Infineon based on the SP37 [3]. Section 6.1.6 describes this module in detail.

For test phase two this module was connected by two power supply cables to the energy harvesting module. Fig. 6.1.4 shows how they were mounted together on the wheel rim.

The receiver module was the UWLink evaluation board [5] based on the TDA5320 chip from Infineon. It can be connected via USB to a PC and was used in conjunction with a simple SP37 evaluation GUI, again provided and developed by Infineon.

Since the wireless link to the TPMS demoboard was not always reliable, the receiver board was mounted near the car wheel case and connected via an USB cable to a laptop.

# 7. Results and Discussion

This chapter presents und discusses the results of the car-tire energy harvester tests. These tests were divided in two phases, a first stage where the voltage and power range was determined and a second with an actual TPMS. Both setups with all involved components are described in chapter 6.

All test drives were recorded with a GPS-logger application running on a common smartphone. The logging interval was set to 1 s. Thus the car speed could be calculated and exported with an adequate GPS evaluation software on a PC.

## 7.1. Test phase one

For this stage tire prototype one was used with rivet connections and lightweight cables. The capacitor size was 10 µF. Furthermore, the measurement voltage divider was continuously active. For images and a more detailed description see section 6.1.2.

Fig. 7.1.1 shows the measured capacitor voltage and the car speed during the first test drive. Two stops at crossroads can be seen during which the capacitor got discharged. From this figure both the capability and the problems of the implemented prototype can be derived.

First of all, the achievable voltage is clearly in a suitable range. Already at 30 km/h the capacitor gets charged to 3.75 V (sec. 80) and at 50 km/h even more than 7 V is reached. Due to the fact that the 13 MΩ voltage divider is continuously active, the discharge current is in the range of 100 nA - 600 nA depending on the capacitor voltage. This is a considerable load compared to the estimated total leakage current of the rectifiers (100 nA). Therefore the achievable charging power is in reality higher. Although this may be true, the necessary standby current of a DC/DC converter and TPMS is comparable to the measurement load and thus the executed test can be seen as a realistic operation.

The biggest problem during this and also the following test drives was the mechanical stability of the wire connections between foils and harvesting electronics. Although the foils themself did not show noteable damages, the wires were seriously stressed. Already during the drive a decreasing charging power was seen, e.g. around sec. 260 in fig. 7.1.1. The inspection after the tire dismount showed only three out of eight working foil connections. A broken bottom electrode connection had the greatest impact because it was

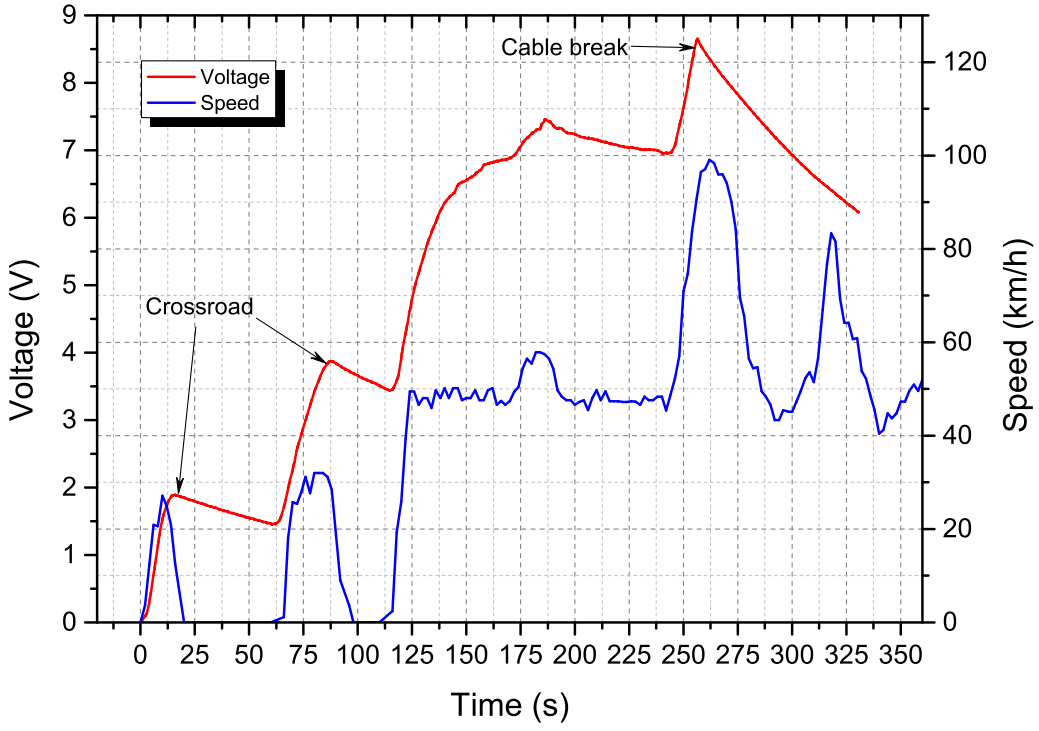


**Figure 7.1.1.** – Test drive with first prototype

shared by four foils. This poses a major problem for the power calculations, since it is not possible to say how many foils were active during the test drive. With this in mind the reached voltages and the following calculated powers should be seen as minimum values.

| Δt [s] | ΔV [V] | P [µW] |
|---|---|---|
| 14.6 | 1.88 | 1.21 |
| 24.7 | 2.38 | 2.56 |
| 29.3 | 2.98 | 5.08 |

**Table 7.1.1.** – Charging power

$$E = \frac{1}{2} \cdot C \cdot U^2$$

$$P = \frac{E_2 - E_1}{\Delta t} = \frac{\frac{1}{2} \cdot C \cdot (U_2{}^2 - U_1{}^2)}{\Delta t}$$

Example:

$$P = \frac{\frac{1}{2} \cdot 10\mu F \cdot ((1.88V)^2 - (0V)^2)}{14.6s} = 1.21\,\mu W$$

Table 7.1.1 shows the calculated mean powers for the three charging steps before sec. 175. The first two steps include the car acceleration and slow down phases while the third step happens during an average speed of ca. 50 km/h.

## 7.2. Test phase two

The prototype for test phase two included the power supply and TPMS like described in section 6.3. To improve the wireless connection, the TPMS receiver was mounted near the wheel case and connected with an USB cable to a laptop inside the car. The storage capacitor was increased to 2x47 µF resulting in a total capacity of 94 µF. Like already

stated in section 6.3.2, the voltage should drop from ca. 4 V to 3 V after a measurement and transmission cycle.

### 7.2.1. Overview

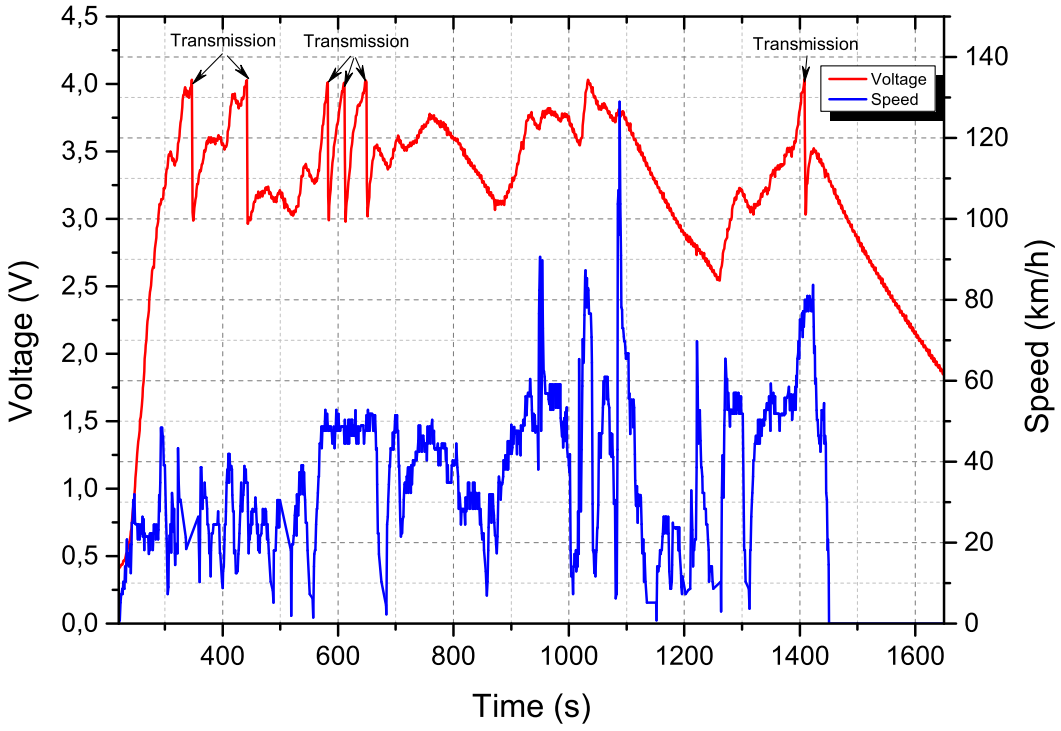


**Figure 7.2.1.** – Test drive with TPMS

Fig. 7.2.1 shows the first of two test drives during this stage with a duration of 25 minutes. This figure gives an overview of the measurement results, the details are discussed in the following sections.

From the measured capacitor voltage the transmission times can be read out. During this drive a total of six frames were transmitted, indicated by the abrupt voltage drop as soon as approximately 4 V is reached. After sec. 1450 the car was stopped and the following discharge curve allows to estimate the standby current of the system. However, again the mechanical stability of the cable connections posed a major problem. It can be assumend that afer sec. 700 the charging power already decreased due to broken connections. Thereafter the voltage does not rise as fast as before at comparable speed.

A subsequent inspection of the tire showed a broken cable set at the electronics connector preventing four foils from contributing to the capacitor charging. Moreover, these free moving cables scratched and destroyed the surface of one other foil, reducing the charging power even further. For the second test drive with this prototype the cables were soldered to the cable lugs leading to seven active foils. Even though that the wire connections

thus were stable, a connector got loose removing again four foils from the electronics. By simply evaluating the capacitor charge curve it is hard to say when exactly the power was reduced by how much. Therefore the calculated powers should be seen as minimum values.

### 7.2.2. Detailed views of transmissions

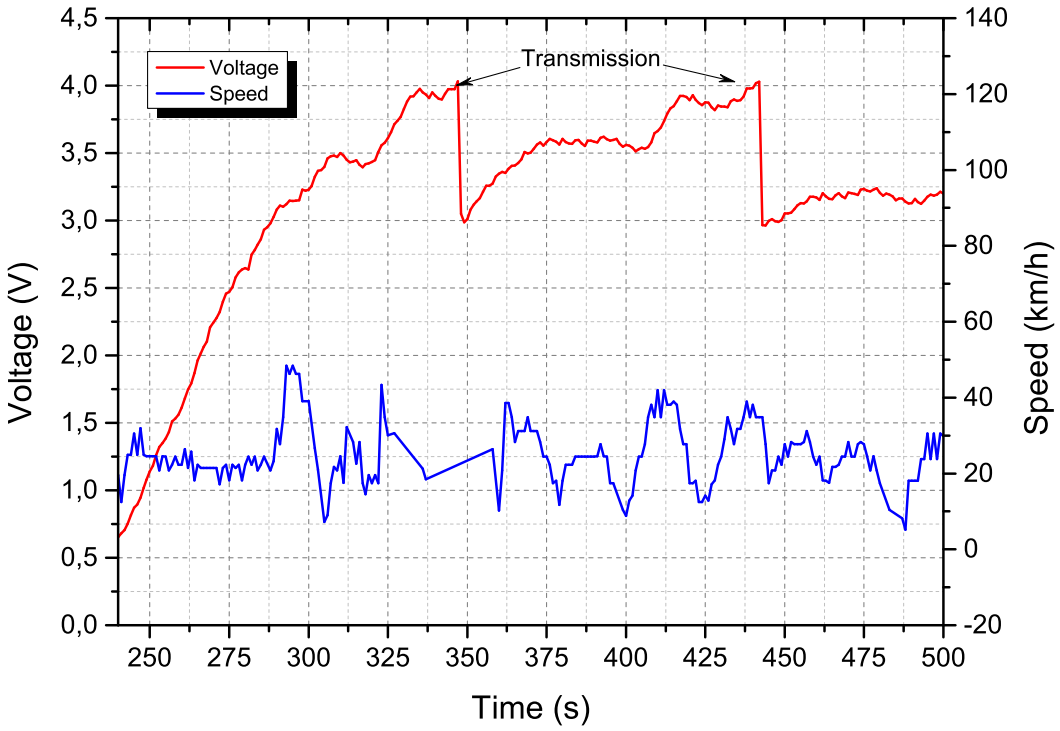


**Figure 7.2.2.** – Transmissions at 30km/h

Fig. 7.2.2 shows the first two frame transmissions at a mean car speed of ca. 30 km/h. It can be seen that the large capacitance (compared to test stage one) gets charged to the point where a first transmission is possible in about two minutes. Since the voltage drops only by 1V after a measurement cycle the charging time for the next cycle is significantly reduced. At sec. 375 the voltage suddenly stops rising althought the car runs at the same speed as before. This can be seen as an indicator that a foil connection got broken. For the next transmission at sec. 440 two short acceleration periods were necessary.

Fig. 7.2.3 depicts a driving period with a more uniform car speed of ca. 50km/h. During 90s three measurements were possible resulting in an average time of 30 s per cycle. It can be seen that after the second transmission the charging power drops, which suggests that another foil got disconnected.

The second test drive during this stage produced the measurement results shown in fig. 7.2.4 where a mean speed of nearly 80 km/h was possible. The time between the

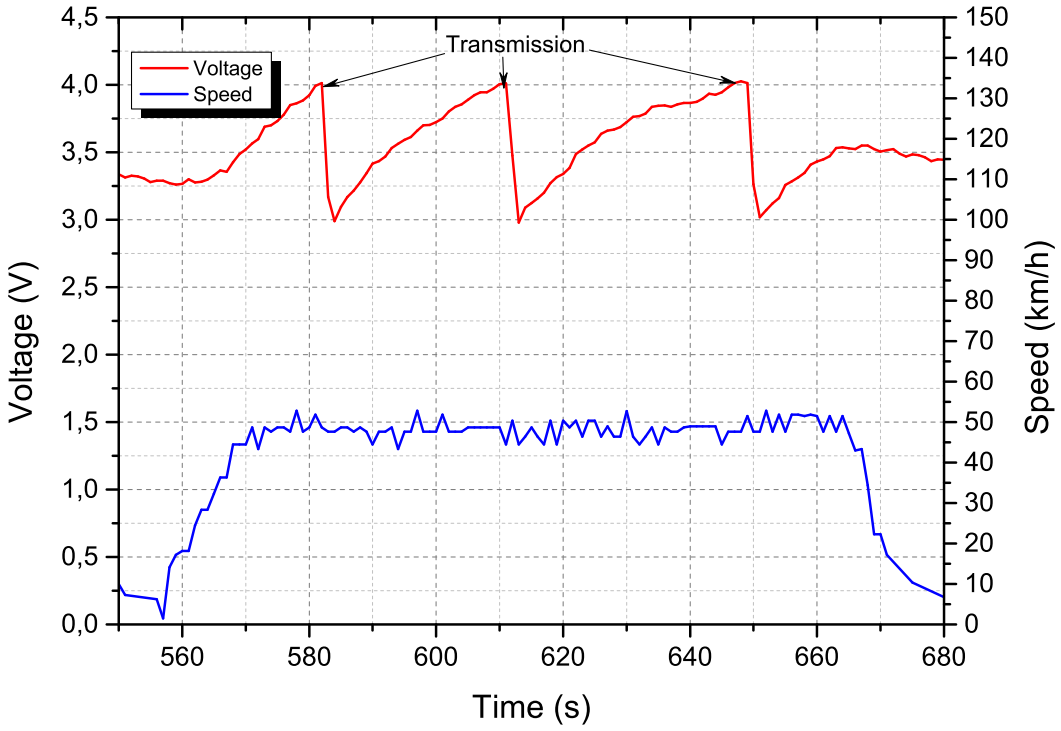


**Figure 7.2.3.** – Transmissions at 50km/h

first and second transmission was reduced to ca. 20 s.

### 7.2.3. Received frames

Table 7.2.1 contains the received frames sent by the TPMS. Although the transmission distance was low (<0.5 m), it was not possible to capture every frame that was sent. Sometimes only a fragment was received. It was not possible to find out the exact cause of this behaviour, but two possible reasons are:

- The TPMS antenna on the demo board is implemented as a PCB track. According to Infineon a wire spring is used in commercial devices. Other TPMS manufacturers use e.g. the tire valve as antenna.
- The sender and receiver were not configurated by software to the optimum. Since both software parts were developed and provided by Infineon it was not possible to verify this assumption.

Nevertheless, it was possible to receive enough frames to verify the measurements done by the TPMS. The supply voltage is near the expected value of +2.5 V, like regulated by the LTC3588-1 power supply. The variation over the six measurements is smaller than 0.5%. The tire pressure is an absolute value, i.e. the air pressure of ca. 100 kPa has to be subtracted. The tire pressure was set to approximately 2.5 bar but not measured

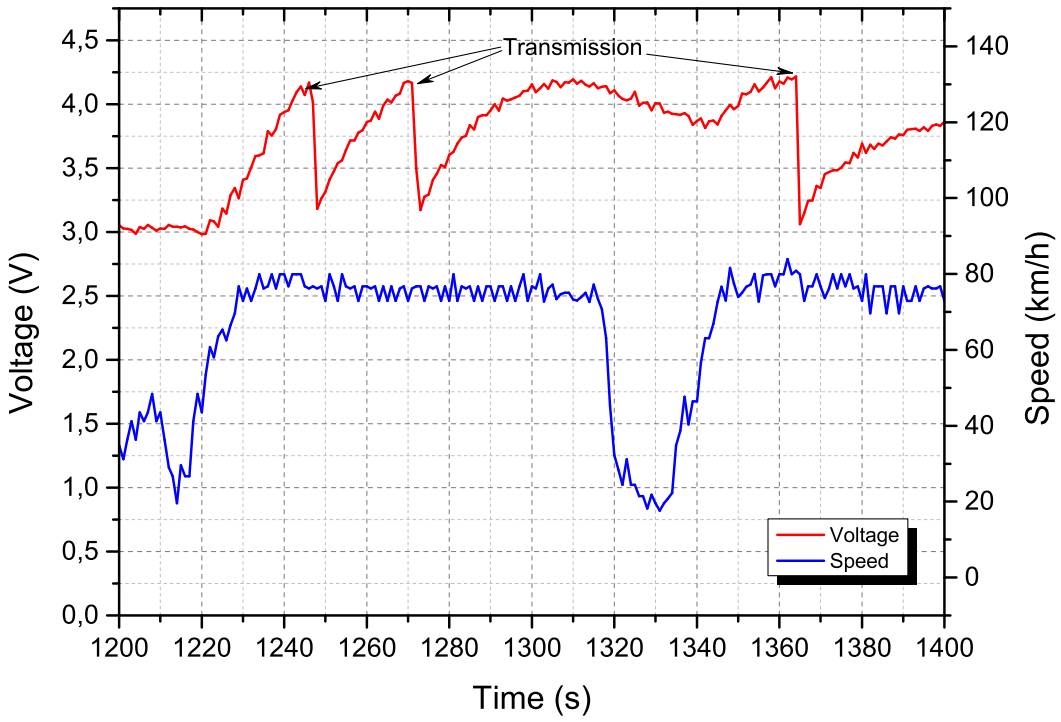


**Figure 7.2.4.** – Transmissions at 80km/h

| Drive nr. | Frame text |
|---|---|
| 1 | RF-Frame; 0x16;0x25; 0x4F;0x1D; |
| 1 | RF-Frame; 0x16;0x39; 0x4F;0x5F; (355,56kPa;2539,88mV) |
| 1 | RF-Frame; 0x16;0x39; 0x4F;0x1D; (355,56kPa;2531,62mV) |
| 2 | RF-Frame; 0x17;0x13; 0x4E (369,19kPa) |
| 2 | RF-Frame; 0x17;0x52; 0x4F;0x3E; (373,12kPa;2535,75mV) |
| 2 | RF-Frame; 0x17;0x5E; 0x4F;0x1D; (373,88kPa;2531,62mV) |

**Table 7.2.1.** – Received frames

exactly. The received values are consistent among the two test drives respectively and seem reasonable.

All in all it can be assumed that the batteryless TPMS worked reliable.

### 7.2.4. Charging power

Table 7.2.1 shows the calculated charging power for ten periods of relatively stable car speed during the two test drives of test phase two. The tire deformation frequency in Hz was derived from the diagram in fig. 7.2.5 where the relation to the car speed in km/h is shown. As circumference 1983 cm was assumed, based on the used tire (205/60/R16).

Observing the calculated powers it must be remembered that the number of actually active foils is not known. The followup examination of the tire showed up to five broken

| v [km/h] | P [µW] | P [µW/Hz] |
|---|---|---|
| 30 | 6.13 | 1.46 |
| 30 | 3.67 | 0.87 |
| 30 | 3.59 | 0.85 |
| 50 | 13.72 | 1.96 |
| 50 | 12.53 | 1.79 |
| 50 | 9.88 | 1.41 |
| 75 | 17.40 | 1.65 |
| 75 | 15.32 | 1.45 |
| 80 | 11.75 | 1.05 |
| 80 | 13.12 | 1.17 |

**Table 7.2.2.** – Calculated charging power

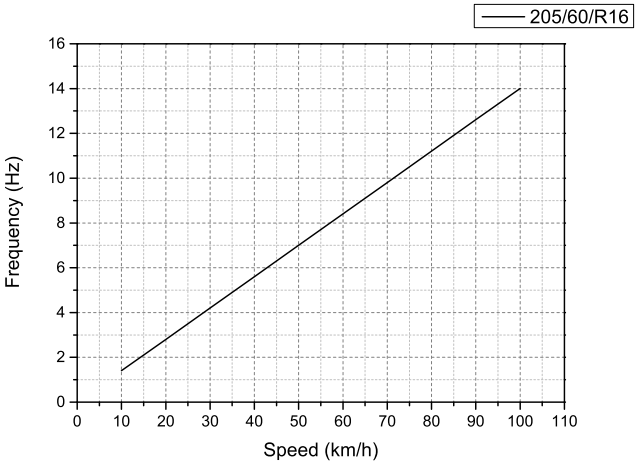


**Figure 7.2.5.** – Tire speed in Hz

connections and unfortunally it was not possible to determine when exactly the power reduction occurred. Furthermore, the charging power is voltage dependent like shown in the simulation results of the rectifier circuits in section 5.2.4. Therefore the calculated values should be seen only as reference points.

From these ten measurements an average power per tire rotation of 1.37 µW/Hz can be calculated.

## 7.2.5. Standby current

The average standby current of 670 nA is consumed by the rectifiers, the power supply and the TPMS. This calculation is based on two discharge curves during a stop time of 234 s and 139 s. Again, this value should be seen as reference point, since the standby current is voltage dependent too.

The voltage measurement system was improved for the second test phase by activating the measurement path only for a short time during the ADC measurement. This reduced the load current to ca. 30 nA which is comparable to the leakage current of the rectifier circuit (ca. 80 nA).

To sum up, the overall standby current lies in the expected range, given a typical power supply quiescent current of 450 nA [11].

# 8. Summary and Outlook

## 8.1. Summary

In this work a practical approach to piezoelectric energy harvesting was shown. Chapter 1 presented a short introduction with focus on the recent and current development of the field. Although the area of piezoelectric energy harvesting has a relatively short history, the different examples of practical applications predict a promising future development. The until now achieved generator powers are of course quite low compared to e.g. devices using the sun or the wind as energy source. Nevertheless, in many situations piezoelectric elements are the key components to produce the necessary power needed. Therefore, the development of novel materials is highly appreciated to further improve efficiency as well as to extend the application area. PyzoFlex, described in detail in chapter 2, is an example for such a step towards large scale and low cost energy harvesting. Additional benefits like a possible application as sensor make this technology even more interesting.

The practical suitability of a piezoelectric device for energy harvesting depends highly on its properties and behaviour. Hence, the given material was analyzed thoroughly, which is described in chapter 3. With the results in mind several use cases in the automotive environment were discussed in chapter 4. To leverage the advantages of the high flexibility and easy scalability a design for random or low frequency mechanical vibration was proposed. Consequently, it was determined that for several reasons the application inside a car tire represents a promising use case. One reason is e.g. that tire pressure monitoring systems became mandatory throughout the EU since November 2014 and therefore a batteryless solution would have a high impact on the industry.

The goal of the practical part of this work was therefore to develop a prototype of a batteryless TPMS using the given piezoelectric foils. In order to achieve an adequate output power and system design the necessary electronic circuits were simulated and analyzed in chapter 5. It was shown that efficient power management and rectifiers are key components of a self-sustained system. Furthermore, it was discussed that circuits with higher output power are not always the best solution for a given application.

Chapter 6 described the buildup and working principle of the developed car-tire energy harvesting prototype. It consists of a tire equipped with PyzoFlex foils, necessary cabling and a rim-mounted electronic device. This device harvests and stores the produced energy and is capable to monitor and transmit wirelessly the storage capacitor voltage value. A

TPMS provided by Infineon was used to prove the practical suitabilty of the developed system.

Finally, chapter 7 showed the results of several test drives with the developed prototype. Apart from problems with the mechanical stability of the wire connections the prototype provided good results. Even with only three to eight 68 $cm^2$ foils it was easily possible to deliver enough energy for a proper TPMS operation. Charging times of well below two minutes for one measurement cycle at a speed of 30 km/h were observed. At 50 km/h already less than 30 s of charging was necessary. Given the comparable easy manufacturing process of PyzoFlex (screen printing) larger foil areas and thus higher output powers are of course feasible.

Therefore it can be concluded that from the point of view of output power a batteryless TPM system based on PyzoFlex is easily possible. What challenges remain and how the next steps for a improved system could look like is discussed in the following section.

## 8.2. Future work

The next steps for further research and development of PyzoFlex foils for piezoelectric energy harvesting can be divided in two categories: a general one regarding the foil properties as well as fundamental considerations and a category for the application in car tires.

### 8.2.1. General

- A key point in evaluating the charge generation is an adequate test setup. This setup should make it possible to apply a reproducible mechanical deformation. Additionally, different modes are interesting like variable frequency or fixation of the foils. As a result, foils with different size, thickness, substrates etc. could be compared.
- The thickness of the polymere layer is an important parameter that changes the capacity and charge output of the foil. Therefore, this property should be analyzed and optimized for energy harvesting. For example, a thicker PVDF layer would lead to a lower capacity and presumably higher voltage but lower charge generation. The understanding of these relations can help significantly to improve the interface circuit.
- Similarly the used substrate has an influence on the capacity. It was observed, that thinner PET substrate lowered the capacity of a foil compared to one with the same size but thicker substrate. Again, this could be a paramter to adjust for improving the energy output.
- If feasible, double or even multilayer foils would be another helpful feature to increase energy output.

- For the prototype the connections from the foil electrodes to the harvesting electronics were done with rivets or screws. Some sample measurements showed significant variations in the contact resistance. It would be desireable not only to improve mechanical stability but also lowering the contact resistance by trying other materials or contacting methods.
- Like the piezoelectric layer also the top and bottom electrodes can be altered or even exchanged with other materials. Since the carbon top electrode showed a resistance in the range of 100 Ω to kΩ per cm it can be assumed that some improvement in this area is possible.
- On the electronics side clearly a more efficient rectifier circuit is important. Depending on the application and power output even active rectification is thinkable. Since many research is ongoing in this area it should be possible to find a more efficient solution. Of course this is always application dependent (size and/or mass constraints).

### 8.2.2. Application in car tires

- To improve the power output of the applied foils several measures are possible. The most valuable would be to simulate and analyze the tire deformation in detail to gain knowledge about the exact behaviour. Consequently, the foil size and position could be optimized, e.g. by trying to mount the foils on the tire sidewalls.
- The next development, probably improving two issues at a time, would be to print a foil with equal size of the tire inner surface. Doing this, it has to be ascertained that the active areas are separated, like discussed in section 3.4. Furthermore, dedicated printed tracks could lead to one common contact point and replace the cables used in the prototype tire. These steps would improve the energy output significantly and have the potential to solve the cable break problem encountered during the first prototype drives.
- A promising research area is the combination of the sensor and energy harvesting properties of PyzoFlex. Since the readout electronics for a touchscreen interface based on this technology already exists, it would be easy to integrate it into another prototype circuit. Depending on the power requirements a self sustained deformation/pressure sensor system is imaginable.
- To develop a real competition to battery powered TPMS solutions the cricital properties (mechanical and temperature stability) as well as the cost issue have to be investigated further.

# Acknowledgments

First of all, I want to thank Dipl.-Ing. Andreas Tschepp and Dr. Martin Zirkl from Joanneum Research. Without their guidance and support this thesis certainly would not have been possible.

I would also like to thank Professor Gunter Winkler for his supervision and all of his advises during this work.

Furthermore, I am also grateful to Ing. Michael Suppan and Mag. Gregor Scheipl for helping me during the prototype construction and test phase.

I would like to offer my special thanks to Dipl.-Ing. Thomas Herndl and his colleagues at Infineon for providing me with necessary hardware and software as well as valuable suggestions.

Finally, I want to say thank you to all of my family and friends for their support.

# A. gatt.xml

```
<?xml version="1.0" encoding="UTF-8" ?>
<configuration>
  <!– 1800: org.bluetooth.service.generic_access –>
  <service uuid="1800" id="generic_access">
    <description>Generic Access</description>
    <!– 2A00: org.bluetooth.characteristic.gap.device_name –>
    <characteristic uuid="2A00" id="c_device_name">
      <description>Device Name</description>
      <properties read="true" const="true" />
      <value>Energy Harvesting Monitor</value>
    </characteristic>
    <!– 2A01: org.bluetooth.characteristic.gap.appearance –>
    <characteristic uuid="2A01" id="c_appearance">
      <description>Appearance</description>
      <properties read="true" const="true" />
      <value type="hex">0100</value>
    </characteristic>
  </service>
  <!– Energy Harvesting Capacitor Voltage Measurement –>
  <service uuid="affeeeee-affe-affe-affe-affeeeeeeeee">
    <description>Capacitor Voltage Measurement</description>
    <characteristic uuid="coffeeee-bada-bada-bada-coffeeeeeeee" id="c_adc_data">
      <description>Capacitor Voltage</description>
      <properties read="true" indicate="true" notify="true"/>
      <value length="40" />
```

```
        </characteristic>
        <characteristic uuid="badf000d-0bad-1bad-2bad-badf0000000d" id="command">
            <properties write_no_response="true" />
            <value length="1" />
        </characteristic>
    </service>
</configuration>
```

# B. hardware.xml

```
<?xml version="1.0" encoding="UTF-8" ?>
    <hardware>
    <sleeposc enable="true" ppm="30" />
    <sleep enable="true" />
    <txpower power="15" bias="5" />
    <script enable="true" />
</hardware>
```

# C. energy_harvester.bgproj

```
<?xml version="1.0" encoding="UTF-8" ?>
<project>
    <gatt in="gatt.xml" />
    <hardware in="hardware.xml" />
    <script in="energy_harvester.bgs" />
    <image out="out.hex" />
    <device type="ble112" />
</project>
```

# D. energy_harvester.bgs

```
# ================================================================
# ADC Measurement for energy harvesting application
# Benjamin Hofer 24.03.2015
# ----------------------------------------------------------------
# ================================================================

# Size of data package sent over bluetooth
const data_size = 40
# ADC measurement frequency
const adc_f = 10
# tmp for storing the ADC result
dim tmp(2)
dim tmp1(2)
# Buffer for BT data
dim data(40)
# Measurement counter
dim msr_nr
# Received command
dim cmd
# Delay for ADC setteling time
dim delay

event system_boot(major, minor, patch, build, ll_version, protocol_version, hw)
  # configure digital outputs (discharge and measure command)
  # Port 0 pin 1 and pin 2 direction to output: 00000110
  call hardware_io_port_config_direction(0, "\x06")
  # Port 0 pin 1 and pin 2 output low
  call hardware_io_port_write(1, "\x0C", $0)
  # begin advertising
  call gap_set_mode(gap_general_discoverable, gap_undirected_connectable)
  msr_nr = 0
end

# Listen for GATT write events
```

```
event attributes_value(connection, reason, handle, offset, value_len, value)
  cmd = value(0:1)
  # Stop measuring command
  if cmd = 0 then
  # Stop measuring by stopping the timer with a last single shot
    call hardware_set_soft_timer(1024, 0, 1)
    # Port 0 pin 1 and pin 2 output low
    call hardware_io_port_write(0, "\x06", $0)
  end if
  # Start measuring
  if cmd = 1 then
    # Start timer for ADC measurement interval
    call hardware_set_soft_timer(32768/adc_f, 0, 0)
    # Port 0 pin 1 and pin 2 output low
    call hardware_io_port_write(1, "\x06", $0)
  end if
  # Discharge Capacitor
  if cmd = 2
    # Set port 0 pin 2 to high and pin 1 to low => short circuit capacitor, di
    call hardware_io_port_write(1, "\x06", "\x04")
  end if
end

event hardware_soft_timer(handle)
  if cmd = 1
    # Connect ADC to capacitor
    call hardware_io_port_write(0, "\x02", "\x02")
    # Insert delay for ADC settling time
    delay = 0
    while delay < 5
      delay = delay + 1
    end while
    # Start ADC measurement: input A0, 12 Bit, internal 1.24V reference
    call hardware_adc_read(0, 3, 0)
  else if cmd = 0
    # No measuring
    msr_nr = 0
  end if
end

event hardware_adc_result(input, value)
  # Disconnect ADC, do not short circuit capacitor
```

```
    call hardware_io_port_write(1, "\x02", "\x00")
    # Realign ADC result for better readability
    tmp1(0:2) = value >> 4
    tmp(1:1) = tmp1(0:1)
    tmp(0:1) = tmp1(1:1)
    # Append measurement to data buffer
    data((msr_nr*2) : 2) = tmp(0:2)
    # Increase measurement counter
    msr_nr = msr_nr + 1
    # Send results over BT when buffer is full
    if msr_nr = data_size/4 then
      call attributes_write(c_adc_data, 0, data_size, data(0:data_size))
      msr_nr = 0
    end if
  end

  event connection_disconnected(handle, result)
    # connection disconnected, resume advertising
    call gap_set_mode(gap_general_discoverable, gap_undirected_connectable)
  end
```

# List of Abbreviations

µC microcontroller

ADC analog-to-digital converter

ASK amplitude-shift keying

BR bridge rectifier

ECU electronic control unit

EH energy harvesting

FSK frequency-shift keying

GATT Generic Attribute Profile

GPS Global Positioning System

GUI graphical user interface

LCR inductance, capacitance, resistance

MEMS microelectromechanical system

MLCC multi-layer ceramic capacitor,

MOSFET metal–oxide–semiconductor field-effect transistor

NASA National Aeronautics and Space Administration

P-SSHI parallel switch harvesting on inductor

PCB printed circuit board

PET polyethylene terephthalate

PVDF polyvinylidene fluoride

PVDF-TrFE polyvinylidene fluoride trifluoroethylene

PZT lead zirconate titanate

RF radio frequency

SDK software development kit

SMU source measure unit

SSHI switch harvesting on inductor

SSHI switch harvesting on inductor

TEG thermoelectric generator

TPMS tire pressure monitoring system

USB Universal Serial Bus

VD voltage doubler

# List of Figures

# List of Tables

# Bibliography


[1] National Aeronautics and Space Administration. Bringing thunder and lightning indoors. https://spinoff.nasa.gov/Spinoff2005/ch_5.html, 2005. Accessed: 2015.07.01.

[2] Continental AG. Contiseal™:the self-sealing standard production tyre from continental. http://www.continental-tires.com/www/tires_de_en/themes/car-tires/link-contiseal.html. Accessed: 2015.06.19.

[3] Infineon Technologies AG. Sp37-main interiors. http://www.infineon.com/cms/de/product/sensor-ics/tire-pressure-sensors/sp37-main-interiors/channel.html?channel=db3a30433899edae0138b91cd6ba6180. Accessed: 2015.06.19.

[4] Infineon Technologies AG. Sp370-25-106-0. http://www.infineon.com/cms/de/product/sensor-ics/tire-pressure-sensors/SP370-25-106-0/productType.html?productType=db3a304430f67fc00131419ae62d1e25. Accessed: 2015.06.19.

[5] Infineon Technologies AG. Uwlink. http://www.infineon.com/cms/de/product/rf-and-wireless-control/wireless-control/development-tooling/uwlink/channel.html?channel=db3a30432ac1eb91012ad23a5c0904a7. Accessed: 2015.06.21.

[6] S. Ben-Yaakov, S. Ben-Yaakov, N. Krihely, and N. Krihely. Resonant rectifier for piezoelectric sources. volume 1, pages 249–253 Vol. 1. IEEE, 2005.

[7] E. Bischur and N. Schwesinger. Energy harvestingfrom floor using organic piezoelectric modules. pages 1–4. IEEE, 2012.

[8] Yu-Yin Chen, D. Vasic, D. Vasic, F. Costa, F. Costa, Wen-Jong Wu, C. K. Lee, and C. K. Lee. Self-powered piezoelectric energy harvesting device using velocity control synchronized switching technique. pages 1785–1790. IEEE, 2010.

[9] East Japan Railway Company. Demonstration experiment of the "power-generating floor" at tokyo station. http://www.jreast.co.jp/e/development/press/20080111.pdf, 01 2008. Accessed: 2015.07.01.

[10] AVX Corporation. Trj series professional tantalum chip capacitor. http://www.avx.com/docs/Catalogs/trj.pdf, 04 2014. Accessed: 2015.06.08.

[11] Linear Technologies Corporation. Ltc3588-1 - nanopower energy harvesting power supply. http://www.linear.com/product/LTC3588-1. Accessed: 2015.06.10.

[12] Linear Technologies Corporation. Ltspice iv. http://www.linear.com/designtools/software/. Accessed: 2015.06.09 Used Version: 4.21x, Sep. 26 2014.

[13] Nazar Fadhil, Dleer Saber, and Prabir Patra. Energy harvesting using nana scale dual layers pvdf film for blood artery. pages 1–6. IEEE, 2013.

[14] D. Guyomar, D. Guyomar, A. Badel, A. Badel, E. Lefeuvre, E. Lefeuvre, C. Richard, and C. Richard. Toward energy harvesting using active materials and conversion improvement by nonlinear processing. *IEEE Transactions on Ultrasonics, Ferroelectrics and Frequency Control*, 49; 52(4):584–595, 2005.

[15] Y. B. Jeon, R. Sood, J. . Jeong, and S. . Kim. Mems power generator with transverse mode thin film pzt. *Sensors & Actuators: A.Physical*, 122(1):16–22, 2005.

[16] Materials Institute Joanneum Research Forschungsgesellschaft mbH. Energy self sufficient touch-interfaces with pyzoflex®-technology. http://www.joanneum.at/en/materials/research-areas/pyzoflexr/eco-touch.html?print=%252525252525252525252Fproc%252525252525252525252Fself%252525252525252525252Fenviron%252525252525252525255C0. Accessed: 2015.07.02.

[17] Materials Institute Joanneum Research Forschungsgesellschaft mbH. Pyzoflex. http://www.joanneum.at/en/materials/research-areas/pyzoflexr.html. Accessed: 2015.07.01.

[18] Tom J. Kazmierski. *Energy harvesting systems: principles, modeling and applications*. Springer, New York [u.a.], 1. edition, 2011.

[19] J. Kymissis, C. Kendall, J. Paradiso, and N. Gershenfeld. Parasitic power harvesting in shoes. pages 132–139, 1998.

[20] M. Lallart, M. Lallart, L. Garbuio, L. Garbuio, L. Petit, L. Petit, C. Richard, C. Richard, D. Guyomar, and D. Guyomar. Double synchronized switch harvesting (dssh): a new energy harvesting scheme for efficient energy extraction. *IEEE Transactions on Ultrasonics, Ferroelectrics and Frequency Control*, 50; 55(10):2119–2130, 2008.

[21] Mickaël Lallart, Élie Lefeuvre, Claude Richard, and Daniel Guyomar. Self-powered circuit for broadband, multimodal piezoelectric vibration control. *Sensors & Actuators: A.Physical*, 143(2):377–382, 2008.

[22] Jaeyun Lee and Bumkyoo Choi. Development of a piezoelectric energy harvesting system for implementing wireless sensors on the tires. *Energy Conversion and Management*, 78:32–38, 2014.

[23] Junrui Liang and Wei-Hsin Liao. Improved design and analysis of self-powered synchronized switch interface circuit for piezoelectric energy harvesting systems. *IEEE Transactions on Industrial Electronics*, 59(4):1950–1960, 2012.

[24] Altium Limited. Altium designer. http://www.altium.com/altium-designer/overview. Accessed:2015.06.20.

[25] Bluegiga Technologies Ltd. Ble112 bluetooth smart module. https://www.bluegiga.com/en-US/products/ble112-bluetooth-smart-module/. Accessed: 2015.06.20.

[26] Bluegiga Technologies Ltd. Bluegiga bluetooth smart software. https://www.bluegiga.com/en-US/products/software-bluegiga-bluetooth-smart/. Accessed: 2015.06.20.

[27] Panasonic Electronic Devices Co. Ltd. "technical guide of electric double layer capacitors - edition 7.4,". http://industrial.panasonic.com/lecs/www-data/pdf/ABC0000/ABC0000TE5.pdf. Accessed :2015.06.08.

[28] Tayo Yuden Co. Ltd. Multilayer ceramic capacitor catalog. http://www.yuden.co.jp/productdata/catalog/en/mlcc01_hq_e.pdf, 10 2014. Accessed: 2015.06.08.

[29] Noaman Makki and Remon Pop-Iliev. Piezoelectric power generation in automotive tires. http://www.ndt.net/article/ndtcanada2011/papers/40_Makki_Rev1.pdf, 11 2011. Accesssed: 2015.07.01.

[30] G. K. Ottman, H. F. Hofmann, A. C. Bhatt, and G. A. Lesieutre. Adaptive piezoelectric energy harvesting circuit for wireless remote power supply. *IEEE Transactions on Power Electronics*, 17(5):669–676, 2002.

[31] Jangwoo Park, Honggeun Kim, Changsun Shin, Kyungryong Cho, Yongyun Cho, and Kisuk Kim. The effect of switch triggering offset and switch on-time duration on harvested power in synchronized switch harvesting on inductor. *International Journal of Smart Home*, 7(3):207–218, 2013.

[32] a Face® Company PulseSwitch Systems, LC. Lightning switch. http://www.lightningswitch.com/. Accessed: 2015.07.03.

[33] Christian Pylatiuk, Fabian Metzger, Roland Wiegand, and Georg Bretthauer. Kinetic energy scavenging in a prosthetic foot using a fluidic system. *Biomedizinische Technik*, 58(4):353–358, 2013.

[34] Jinhao Qiu, Hao Jiang, Hongli Ji, and Kongjun Zhu. Comparison between four piezoelectric energy harvesting circuits. *Frontiers of Mechanical Engineering in China*, 4(2):153–159, 2009.

[35] Tomáš Zedníček. AVX Corporation Radovan Faltus, Miroslav Jáně. Storage capacitor properties and their effect on energy harvester performance. http://www.avx.com/docs/techinfo/EnergyHarvesting.pdf. Accessed: 2015.06.08.

[36] C. Richard, D. Guyomar, and E. Lefeuvre. Self-powered electronic breaker with automatic switching by detecting maxima or minima of potential difference between its power electrodes, June 7 2007. WO Patent App. PCT/FR2005/003,000.

[37] G. Scheipl, M. Zirkl, A. Sawatdee, U. Helbig, and M. et al. Krause. All printed touchless human-machine interface based on only five functional materials". *Proc. SPIE 8258, Organic Photonic Materials and Devices XIV, 82580P*, 2012.

[38] NXP Semiconductors. Bav199 low-leakage double diode. `http://www.nxp.com/documents/data_sheet/BAV199.pdf`. Accessed: 2015.06.09.

[39] NXP Semiconductors. Bsh103 n-channel enhancement mode mos transistor. `http://www.nxp.com/documents/data_sheet/BSH103.pdf`, 01 1998. 2015.06.20.

[40] R. Shukla, Rahul Shukla, S. A. Qaisar, S. A. Qaisar, A. J. Bell, and Andrew J. Bell. Towards the development of efficient low frequency piezoelectric energy harvesters. pages 1–4. IEEE, 2010.

[41] Stratis Kanarachos Martin Rexeis Stefan Hausberger Richard Smokers Stephan van Zyl, Sam van Goethem. Study on tyre pressure monitoring systems (tpms) as a means to reduce light- commercial and heavy-duty vehicles fuel consumption and co2 emissions. `http://ec.europa.eu/clima/policies/transport/vehicles/heavy/docs/tno_2013_final_report_en.pdf`, 08 2013. Accessed: 2015.07.02.

[42] Avago Technologies. Hsms-280x surface mount rf schottky barrier diodes. `http://www.avagotech.com/docs/AV02-0533EN`. Accessed: 2015.06.09.

[43] R. J. M. Vullers, M. Renaud, R. Elfrink, and R. van Schaijk. Mems based vibration harvesting: Facing the ugly facts. pages 685–688. IEEE, 2013.

[44] Z. Wang, R. Elfrink, R. J. M. Vullers, V. van Acht, M. Tutelaers, S. Matova, J. Oudenhoven, and R. van Schaijk. Large power amplification of a piezoelectric energy harvester excited by random vibrations. pages 106–109. IEEE, 2013.

[45] Xuan Wu, Mitesh Parmar, and Dong-Weon Lee. A seesaw-structured energy harvester with superwide bandwidth for tpms application. *IEEE/ASME Transactions on Mechatronics*, 19(5):1514–1522, 2014.

[46] Jingjing Zhao and Zheng You. Models for 31-mode pvdf energy harvester for wearable applications. *TheScientificWorldJournal*, 2014:893496, 2014.

[47] T. Zimmermann, A. Frey, M. Schreiter, J. Seidel, and I. Kuehne. Mems-based piezoelectric energy harvesting modules for distributed automotive tire sensors. pages 1–4. IEEE, 2012.

[48] M. Zirkl, G. Scheipl, B. Stadlober, P. Hartmann, and M. Haller. Pyzoflex: a printed piezoelectric pressure sensing foil for human machine interfaces. *Proc. SPIE 8831, Organic Field-Effect Transistors XII; and Organic Semiconductors in Sensors and Bioelectronics VI, 883124*, 2013.

[49] Martin Zirkl, Anurak Sawatdee, Uta Helbig, Markus Krause, Gregor Scheipl, Elke Kraker, Peter A. Ersman, David Nilsson, Duncan Platt, Peter Bodö, Siegfried Bauer, Gerhard Domann, and Barbara Stadlober. An all-printed ferroelectric active matrix

sensor network based on only five functional materials forming a touchless control interface. *Advanced materials (Deerfield Beach, Fla.)*, 23(18):2069, 2011.